EUROPEAN COMMISSION

Community Research

SEVENTH FRAMEWORK PROGRAMME

# CARBOWASTE

***Treatment and Disposal of Irradiated Graphite and Other Carbonaceous Waste***

**Grant Agreement Number: FP7-211333**

# - Technical Report (WP 3 Task 3.2) – - CHARACTERISATION OF G2 PILE GRAPHITE - BEFORE AND AFTER IRRADIATION -

Author(s): **J. COMTE – L. GOSMAIN – C. GUY**

Date of issue of this report : October 2010

Start date of project : **01/04/2008** Duration : **48 Months**

| **Project co-funded by the European Commission under the Seventh Framework Programme (2007 to 2011) of the European Atomic Energy Community (EURATOM) for nuclear research and training activities** | | |
|---|---|---|
| **Dissemination Level** | | |
| **PU** | Public | |
| **RE** | Restricted to the partners of the CARBOWASTE project | |
| **CO** | Confidential, only for specific distribution list defined on this document | **X** |

# Distribution list

| Person and organisation name and/or group | Comments |
|---|---|
| W. Von Lensa, CARBOWASTE Project coordinator | |
| G. PINA, Work Package 3 leader | |
| B. Grambow, Work Package 6 leader | |
| L. Petit, EDF | |
| S. Schumacher, ANDRA | |
| M. Firon, CEA | |
| C. Ferry, CEA | |
| P. Thouvenot, CEA | |
| CARBOWASTE beneficiaries. | |
| | |
| | |
| | |
| | |
| | |
| | |
| | |
| | |
| | |
| | |
| | |
| | |
| | |
| | |
| | |
| | |

| CARBOWASTE | | |
|---|---|---|
| **Work package:** 3<br>**Task: :** 3.2 | **CARBOWASTE document no:**<br>CARBOWASTE-1007-D-WP3.Task.2 | **Document type: T**<br>D=Deliverable / M=Minutes / P=Progress report / T=Technical Report |
| **Issued by:** CEA<br>**Internal no.:** Technical report CEA G2 WP3 | | **Document status:**<br>Final |

**Document title**

# Characterisation of G2 pile graphite before and after irradiation

**Executive summary**

This document describes the characterisation of solids on virgin and irradiated graphite samples from the G2 UNGG reactor. The purpose of those analyses is to grasp the essential physical properties of graphite in studies for understanding the behaviour not only of graphite within a reactor in operation, but also of radionuclides under disposal conditions.

The characterisation studies refer to density, porosity and pore-water-distribution measurements, as well as characterisation activities by X-ray diffraction of virgin and irradiated graphite samples. Other characterisations by Raman spectroscopy were also made on G2 virgin samples pending the availability of measurements on irradiated samples.

The evolution of those parameters during the irradiation of the G2 reactor will be addressed.

**Revisions**

| Rev. | Date | Short description | Author | Internal Review | Task Leader | WP Leader |
|---|---|---|---|---|---|---|
| | | Issue | Name, Organisation | Name, Organisation *Signature* | Name, Organisation *Signature* | Name, Organisation *Signature* |
| 00 | 10/2010 | First issue | COMTE CEA | GUY CEA | | PINA CIEMAT |
| | | |  |  | | |

# Table of Content

# 1 Introduction

Thanks to its mechanical, thermal and neutronic properties, graphite has been used as a moderating agent in graphite-moderated gas-cooled reactors (*Uranium Naturel Graphite Gaz : UNGG*).

In the framework of studies on the disposal of graphite waste resulting from the UNGG reactor system, it is necessary to provide scientific data on the behaviour of long-lived radionuclides $^{36}Cl$ and $^{14}C$, with due account of their mobility in the geological environment in relation to their long radioactive half-life.

A R-D programme was proposed with a view to studying and quantifying the release mechanisms of those radionuclides in water. A bibliographical study was summarised[1]. The release of radionuclides in solution depend on many physico-chemical processes, as follows :

- the input of reactants (water) on radionuclide sites;
- the solubilisation of radionuclides,
- the transport of radionuclides in solution through the graphite pores towards the solution.

The characteristics of the porous graphite material constitute essential parameters that will largely influence the physico-chemical processes controlling the release of radionuclides in solution.

In that framework, samples of the G2 reactors were characterised in different CEA laboratories : Laboratory of Chemical and Radiochemical Analyses (*Laboratoire d'analyses chimiques et radiochimiques* –DEC/SA3C/LARC), with the support of the Assessment and Destructive Characterisation Laboratory (*Laboratoire d'expertise et de caractérisation destructive* – DSN/SEEC/LECD), and at the Physico-chemical Characterisation Laboratory for Irradiated Materials (*Laboratoire de caractérisations physico-chimiques des matériaux irradiés* – DMN/SEMI/LPCMI).

This report presents the results of the physical characterisations of virgin and irradiated stack-graphite samples collected from the G2 reactor, notably the measurements of geometric density, porosity and pore distribution, as well as the characterisations by X-ray diffraction and Raman spectroscopy.

The first part of this report summarises bibliographical data, the rationale behind the selection of samples and their preparation for characterisation purposes. The second part deals with experimental results, which includes various measurements, such as density, porosimetry by helium and bromobenzene pycnometry, porosimetry measurements by mercury intrusion and lastly, microstructural characterisations by X-ray diffraction and Raman spectroscopy.

# 2 Sample selection and preparation

In the framework of the study on radionuclide behaviour in irradiated graphite within an aqueous medium, two different reactors were investigated: G2 and SLA2. The selection of both reactors is justified by the different characteristics of pile graphite and the operating conditions of the reactors in particular, as follows :

- the nature of the coke and of initial impurities,
- the neutronic and thermal powers, the $CO_2$ pressure, the thermal background of graphite during the operation of the reactor, and the presence of carboxyhydrogenated deposits.

Table 1 recalls the main differences between the G2 and SLA2 reactors. It should be noted that their selection is also justified by the fact that we have a sufficient number of non-irradiated and irradiated graphite samples whose thermal and neutronic backgrounds are very well known.

| Reactor | G2 | SLA2 |
|---|---|---|
| Divergence date | July 1958 | June 1971 |
| Shutdown date | February 1980 | May 1992 |
| Thermal power (*MW*) | 260 | 1,700 |
| $CO_2$ pressure (*MPa*) | 1.5 | 28.5 |
| Mass of graphite pile (t) | 1,500 | 2,200 |
| Temperature of graphite during operation | 140-380°C | 240-470°C |
| Nature of graphite (*core*) | "Special" Grade-A coke | MgF purified Lima coke |
| Carbonaceous deposits | "Low" | "High" |
| Density of graphite | 1.71 | 1.684 |

TABLE 1: CHARACTERISTICS OF THE G2 AND SLA2 REACTORS

# 3 Summary of knowledge on G2 graphite

## *3.1.Acquired data on virgin graphite*

The pile graphite in the G2 reactor, whose content is based on "Special" Grade-A and Lockport-L cokes, consists of 14,092 parallelepipedic bricks with a section measuring 200 mm square over a maximum length of 1,500 mm. Laid down horizontally to form a prism measuring 9.05 m long by 9.4 m high and 9.53 m wide, the bricks are perforated to let 1,200 channels pass through[2]. The reactor contains three grades of graphite distributed among four separate zones (Figure 1). The active cylinder of the G2 reactor consists of "Special" Grade-A graphite, which has been impregnated once and purified, and whose density is generally said to be 1.71[3].

In J. Rappeneau's 1959 report[4] summarising the density measurements made during the G2-G3 graphite-production campaign, densities were measured mainly not only on five bars selected at random from each industrial batch and intended for cross-section measurements, but also on a certain number of virgin bars[5]. As a reminder, an industrial batch used to include about 190 bars measuring 225 $mm^3$ square by 1,500 $mm^3$ long. For the sake of capture and geometric-density cross-section measurements in the ZOÉ pile, samples were recut within a section of the bar into pieces weighing between 3 and 5 kg[6].

The bulk density of G2 graphites consisting of "Special" Grade-A ("batch") is 1.703 with a dispersion of 0.01 (n=41, K=1), but with a value range between 1.65 and 1.73. The results obtained on sub-samples, call "barreaux balançoire" are very close with an average value of 1.698, whereas the density of virgin bars before rework is 1.72 on average (789 values, some of which probably result from mixed batches). The bulk-density discrepancy between the virgin graphite bars and the same machined graphite bars reaches 0.02.

A similar tendency, although less significant, is observed on Lockport graphite.

| **Special-coke-based graphite** | | | | | **Lockport-coke-based graphite** | | | | |
|---|---|---|---|---|---|---|---|---|---|
| **Type** | **Density** | **Devia t. (σ)** | **Interval** | **Number of values** | **Type** | **Density** | **Gap (σ)** | **Interval** | **Number of values** |
| ***Barreaux balançoires*** | 1.698 | 0.024 | 1.60-1.78 | 235 | ***Barreaux balançoires*** | 1.672 | 0.025 | 1.59-1.72 | 78 |
| Batches | 1.703. | 0.01 | 1.65-1.73 | 41 | Batches | 1.670 | 0.013 | 1.65-1.69 | 11 |
| Raw bars | 1.725 | – | – | 789 | Raw bars | 1.680 | | | 247 |
| 33% of values are below 1.70<br>17% % of values are equal to 1.70<br>50% of values are over 1.70 | | | | | 36% of values are below 1.67<br>15% of values are equal to 1.67<br>49% of values are over 1.67 | | | | |

TABLE 2: DENSITY OF G2 VIRGIN GRAPHITE

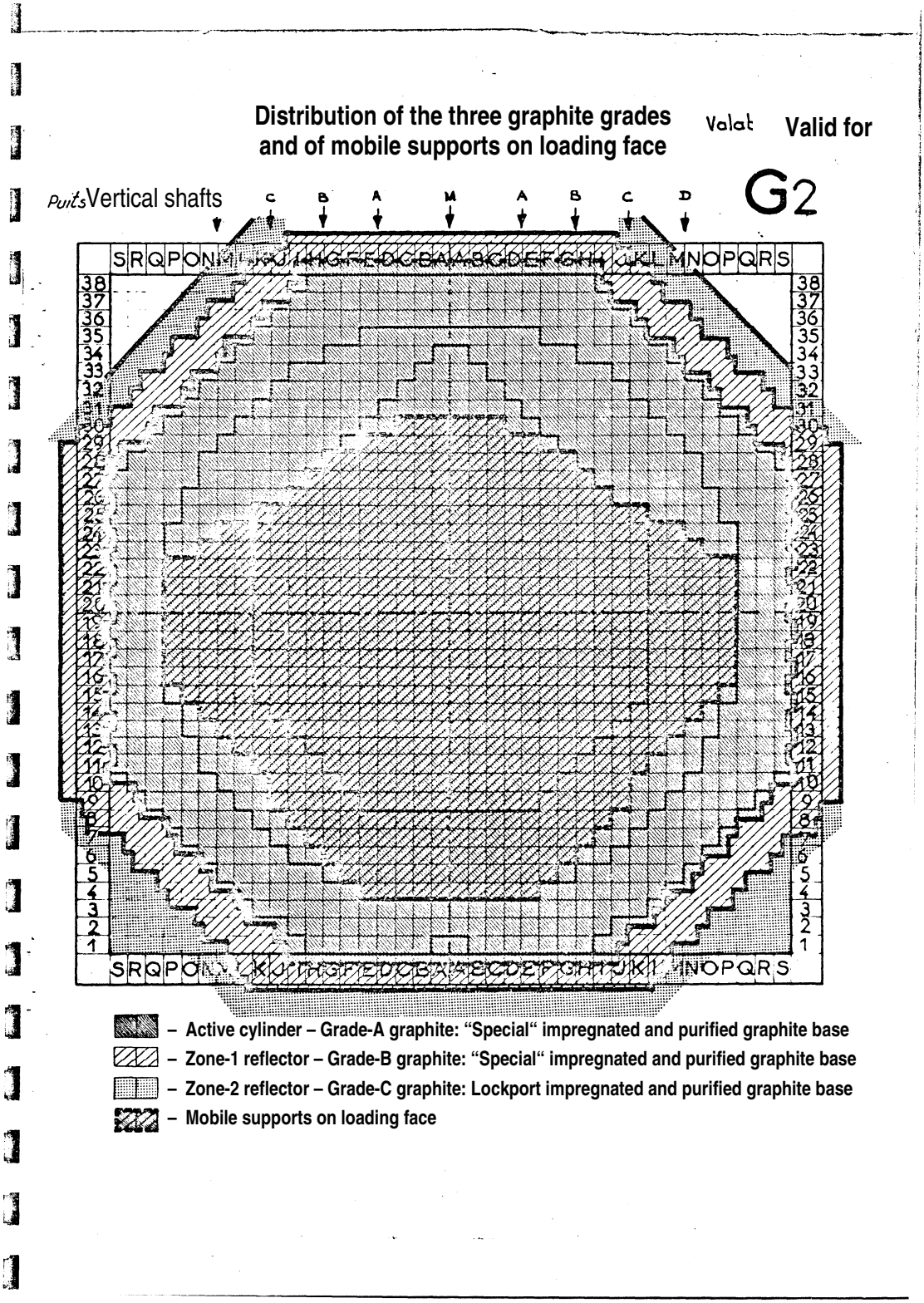


FIGURE 1: DISTRIBUTION OF THE DIFFERENT GRAPHITE GRADES IN THE G2 REACTOR

J. Rappeneau[7] summarises also the parameters that were studied in the development of suitable graphites for nuclear reactors, notably the impact of graphite impregnation on pore density and distribution. Figure 2 shows the evolution of the porosity of a "Special"-coke-based graphite having been submitted to zero (A), one (B) or two impregnations (C). The authors noted that impregnation raises the bulk density of graphite from 1.53 to 1.79 and reduces porosity by acting essentially in the domain of high-radius pores, thus leaving rather intact the porous microstructure. The graphite of the G2 moderator, which has been manufactured with "Special" once-impregnated coke, has a density close to the Grade-B graphite of this study.

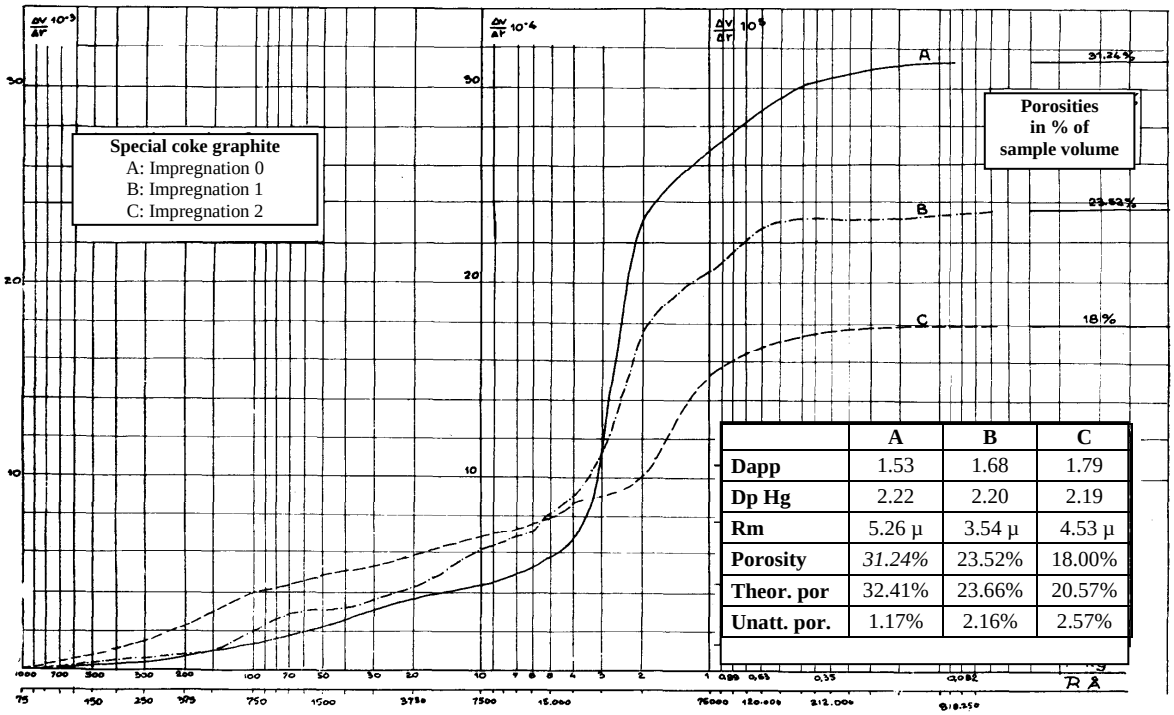


| | A | B | C |
|---|---|---|---|
| Dapp | 1.53 | 1.68 | 1.79 |
| Dp Hg | 2.22 | 2.20 | 2.19 |
| Rm | 5.26 µ | 3.54 µ | 4.53 µ |
| Porosity | *31.24%* | 23.52% | 18.00% |
| Theor. por | 32.41% | 23.66% | 20.57% |
| Unatt. por. | 1.17% | 2.16% | 2.57% |

FIGURE 2: EFFECT OF TAR IMPREGNATIONS: MODIFICATION OF THE POROSITY CURVE

Other parameters, such as mechanical resistances (parallel or perpendicular extrusion-wise), heat-exchange coefficients and capture sections are also available in this document.

Studies on the porous texture of virgin graphites were also conducted on simply impregnated Lockport-coke-based graphite[8] identical to the graphite of the G2 reflector and on Grade-A coke-based graphite close to "Special" Grade-A coke (English) of the G2 moderator. The authors present notably porosity ranges by mercury intrusion (Figures 3 and 4). The main parameters indicated in this study are summarised in Table 3.

| Graphite | Apparent density | Total porosity ($P_t$) | Apparent porosity accessible to Hg ($P_{Hg}$) | Sealed porosity ($Pt$-$P_{Hg}$) | Porosity peaks |
|---|---|---|---|---|---|
| **Lockport L** | 1.691 | 25.38% | 21.42% | 3.96% | 2 µm<br>0.02 µm |
| **Grade A** | 1.788 | 21.09% | 17.17% | 3.92% | 3 µm<br>0.015µm |

TABLE 3: SUMMARY OF MERCURY-POROSITY MEASUREMENTS ON INACTIVE SAMPLES FROM REFERENCE [8]

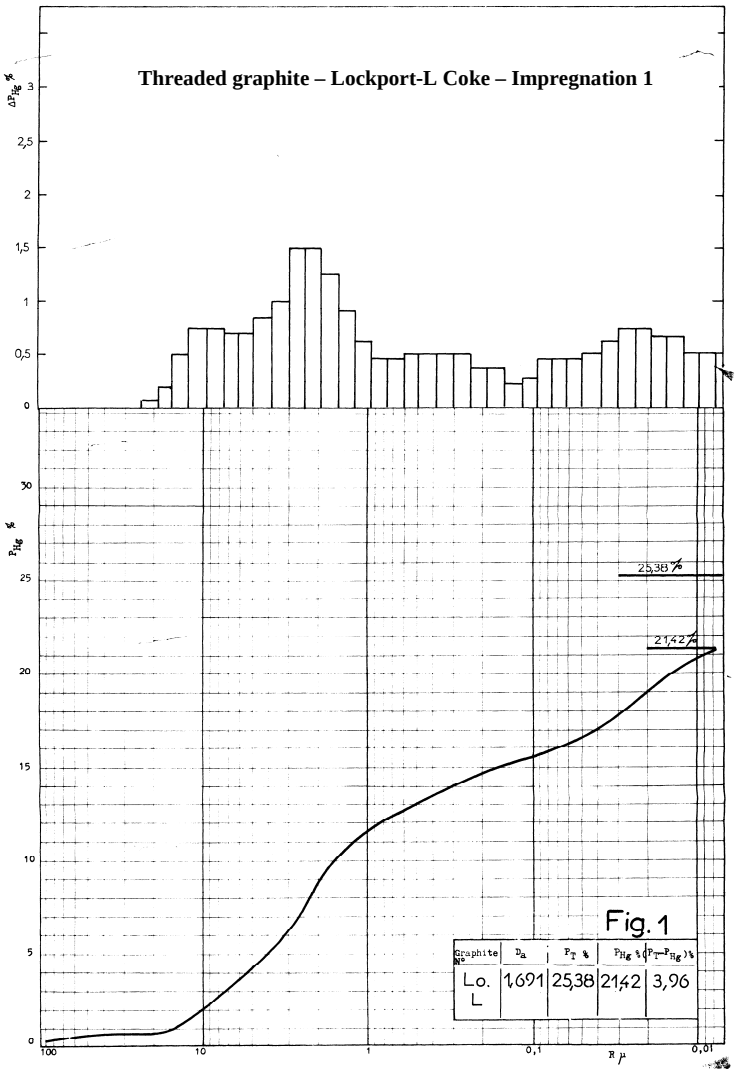


FIGURE 3: MERCURY-POROSITY RANGE FOR SIMPLY IMPREGNATED, BUT NON-IRRADIATED LOCKPORT-L COKE-BASED GRAPHITE

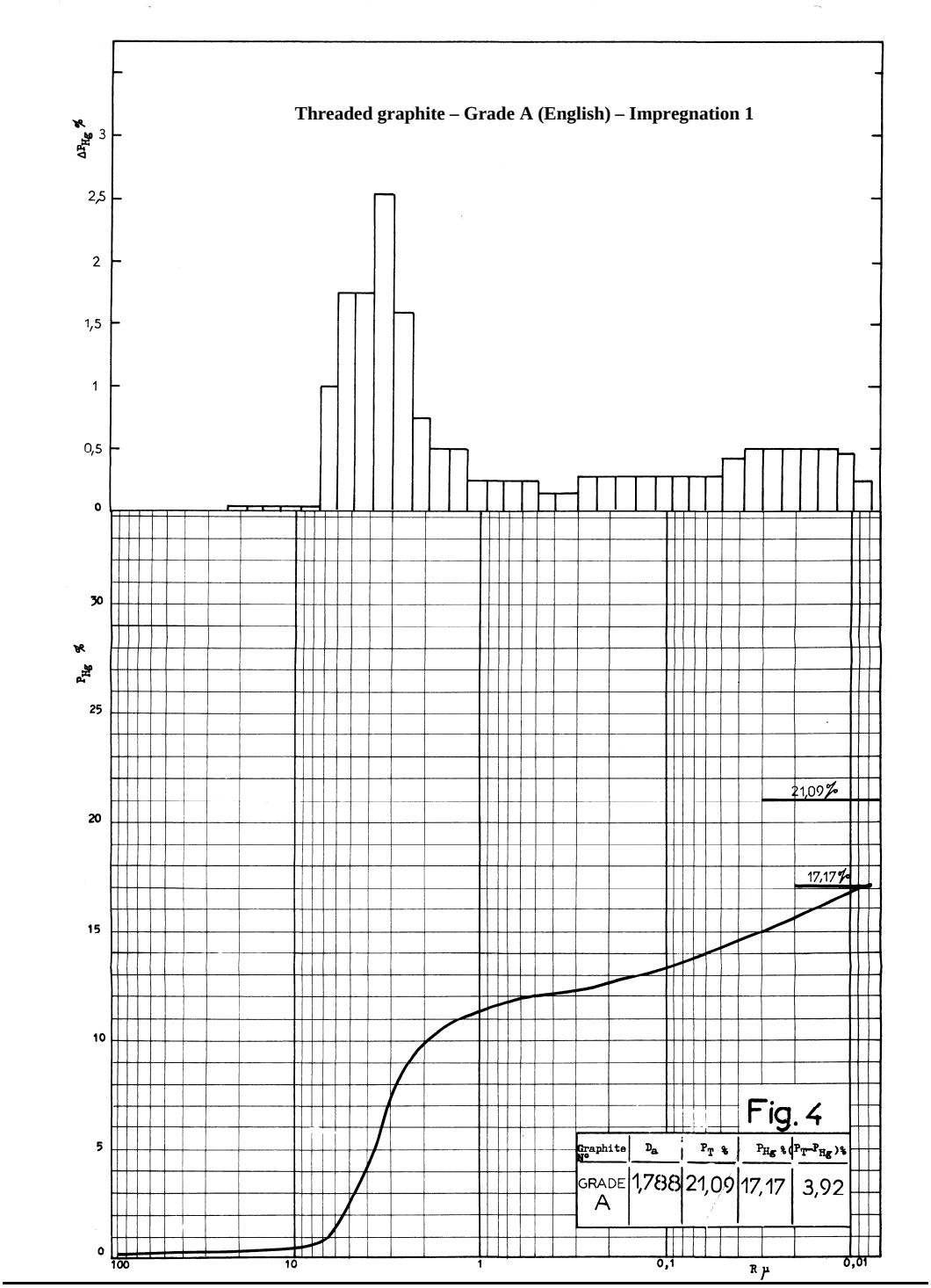


FIGURE 4: MERCURY-POROSITY RANGE FOR SIMPLY IMPREGNATED, BUT NON-IRRADIATED GRADE A-COKE-BASED GRAPHITE CLOSE TO THE SPECIAL COKE OF THE G2 MODERATOR

## 3.2. Acquired data on irradiated graphite

During the operation of the G2 reactor, several cores of small samples were collected notably to monitor graphite wear due to the combined impact of irradiation and temperature. The note referenced C19.05 in DOCMAN provides information on sampling dates and the number of collected samples during the operation (some of those samples are still disposed of in the G2 basements).

Since its shutdown in 1980, the G2 reactor has gone through three coring campaigns, as follows:

– in 1980, axial cores were collected along two channels (central W17A channel and W14P peripheral channel);
– in 1988, a horizontal radial core was collected on 15 cores measuring 80 mm in diameter and a total of 3 m in length; a summary of the coring operations is presented in Reference [9], and
– in 1989, vertical radial cores of the median plane of the reactor were collected over the entire pile graphite (47 cores) in a zone where the neutron flux corresponds to approximately 85% of the maximum reactor flux.

From those three campaigns, there is no sample left from the first two. Only vertical cores are available as samples for new measurements.

During the previous coring campaigns, the collected samples were mostly used for the purposes of a radiological inventory[10] and for leaching and impregnation tests[11] (axial coring). However, certain structural data were measured (density, and more rarely, porosity) and various size-related data were recorded, thus allowing for geometric densities to be calculated[12].

| | Location | Mass (*g*) | Diameter (*mm*) | Height (*mm*) | Calculated density |
|---|---|---|---|---|---|
| **Core 1** | Reflector | 629 | 79 | 80 | 1.60 |
| **Core 2-A** | Reflector | 640.5 | 78 | 80 | 1.68 |
| **Core 2-B** | Reflector | 641.5 | 78 | 80 | 1.68 |
| **Core 3** | Reflector | 623.5 | 78 | 80 | 1.63 |
| **Core 4** | Reflector | 654 | 79 | 80 | 1.67 |
| **Core 5** | Reflector | 653.35 | 79 | 80 | 1.67 |
| **Core 6** | Moderator | 645.5 | 78 | 80 | 1.69 |
| **Core 7** | Moderator | 634 | 78 | 80 | 1.66 |
| **Core 9** | Moderator | 647 | 78 | 80 | 1.69 |
| **Core 10** | Moderator | 619 | 79 | 80 | 1.58 |
| **Core 12** | Moderator | 633 | 78 | 80 | 1.66 |
| **Core 13** | Moderator | 628 | 78 | 80 | 1.64 |
| **Core 14** | Moderator | 643.6 | 78 | 80 | 1.68 |

TABLE 4: DENSITY OF G2 SAMPLES FROM THE 1988 HORIZONTAL RADIAL CORING CAMPAIGN

It should be noted that all recorded data in Table 4 correspond to the reworked semi-cores being used not only for the different leaching tests, but also for impregnation tests with bitumen or epoxy resins[19-11-12].

## 3.3. Summary of existing data

Many studies have been conducted on the graphites of the initial G1 and G2 reactors, notably with regard to the density and porosity measurements during the fabrication of the graphites. However, it is obvious that graphite is a porous material, which is very difficult to characterise, and that a large number of analyses provide robust data that allow for the variability in densities within the graphite to be taken into account.

Many active samples from the G2 reactor were used, but very few of them were fully characterised with regard to the physical properties of the solid. Most of the time, we have access to density levels that are based on the dimensional measurements mentioned in a descriptive objective and not for determining their exact density. On the basis of such data, one may observe that the density of the irradiated samples is often lower than that of virgin graphite. However, those variations seem low and difficult to interpret, due to the measurement methodology and the density variations of virgin graphite.

The lack of data has motivated new measurements to be taken on both non-irradiated and irradiated samples.

# 4 Sample preparation

## *4.1. Inactive samples*

The brick being used as reference for non-irradiated samples was collected from a stock of bricks located under the G2 reactor. It measures 200 mm square and includes two semi-channels measuring 70 mm in diameter and 50 cm in length. Consequently, it results from the cutting of a whole brick measuring 1.5 m in length. It corresponds to the shape of the G2 moderator bricks, which contain a “Special” Grade-A coke base.

Starting with that brick, successive lamellae of about 3 cm in thickness were cut with a cable saw from the LECD and transferred to the different laboratories participating in the programme.

| Lamella | Laboratory | Remarks |
|---|---|---|
| 1° | LPCMI | Whole lamella, then recut (see plan) |
| 2° | SUBATECH | Whole lamella |
| 3° | IPNL | Samples recut in several pieces |
| 4° | LARC | Whole lamella, then recut (see plan) |

TABLE 5: DISTRIBUTION OF GRAPHITE LAMELLAE OF A G2 VIRGIN BRICK

With regard to the LARC and the LPCMI, the initial lamellae were recut with a cable saw in order to obtain different samples for the various tests (see plans in Figure 5).

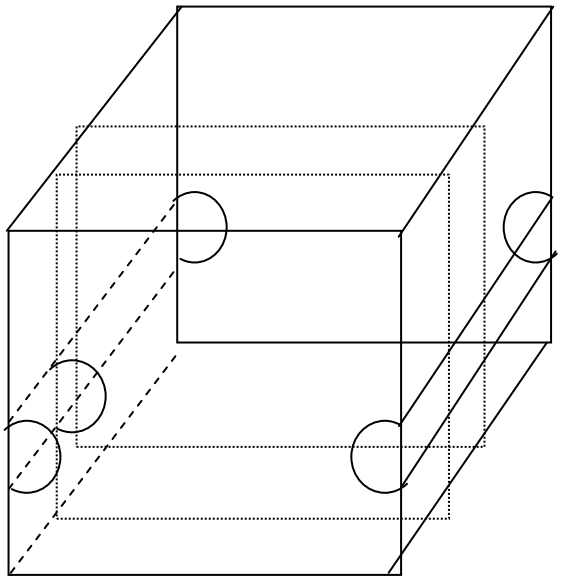

1° - LPCMI
2° - SUBATECH
3° - IPNL
4° - LARC

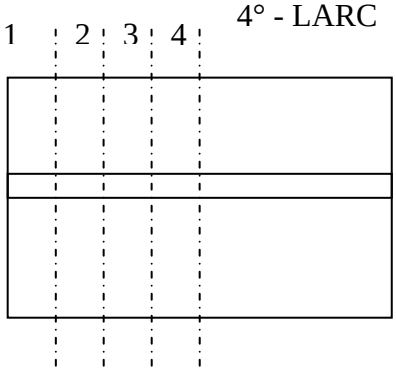


LARC recut

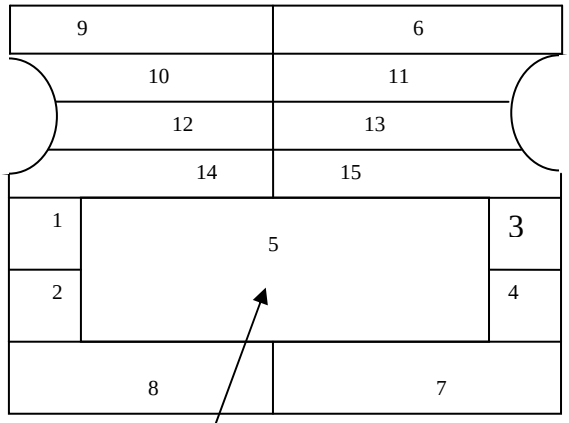


Core samples for leaching tests
and density measurements

LPCMI ***recut***

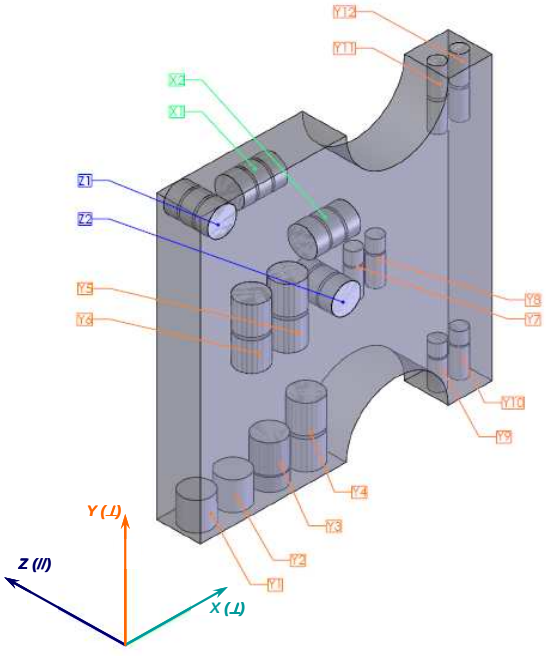


FIGURE 5: CUTTING PLANS OF INACTIVE G2 GRAPHITE BRICK

## 4.2. Active samples

We selected four cores from different parts of the bottom half of the reactor: three from the moderator (Nos. 27, 32 and 42: "Special" Grade-A coke) and one from the reflector (No. 46: Lockport L coke). Hence, we were able to integrate the leaching results of core No. 36 from a previous study[13] to the results that were obtained with the cores selected here. In the end, the five cores were almost equidistant from each other as shown in Figure 6.

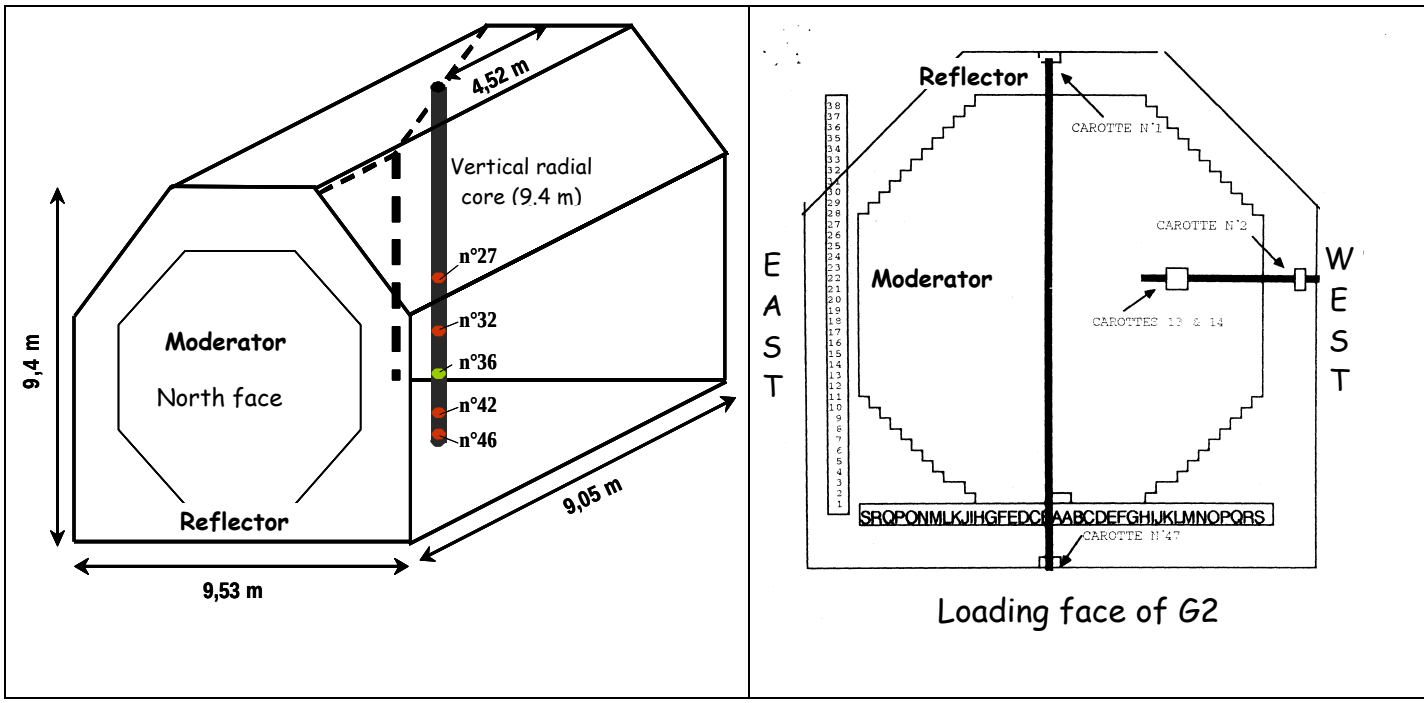


FIGURE 6: REPRESENTATION OF THE G2 REACTOR WITH VERTICAL RADIAL CORING AND SELECTED CORES

Figure 7 shows the temperature distribution of the graphite in the reactor during its operation and the dose mass rate at contact with the vertical graphite cores in relation to the position of the cores in the pile. Table 6 displays the sampling levels and the temperatures of the operating reactor for the selected G2 samples for leaching and characterisation tests.

| Sample no. | Position | Presumed original coke | Sampling level (*m*) | Operating temperature (°C) [14] |
|---|---|---|---|---|
| G2-27 | Moderator | Special coke A | 13.60 | 310 |
| G2-32 | Moderator | Special coke A | 14.60 | 300 |
| G2-42 | Moderator | Special coke A | 16.60 | 280 |
| G2-46 | Reflector | Lockport L coke | 17.40 | <250 |

TABLE 6: SELECTED G2 SAMPLES FOR LEACHING TESTS

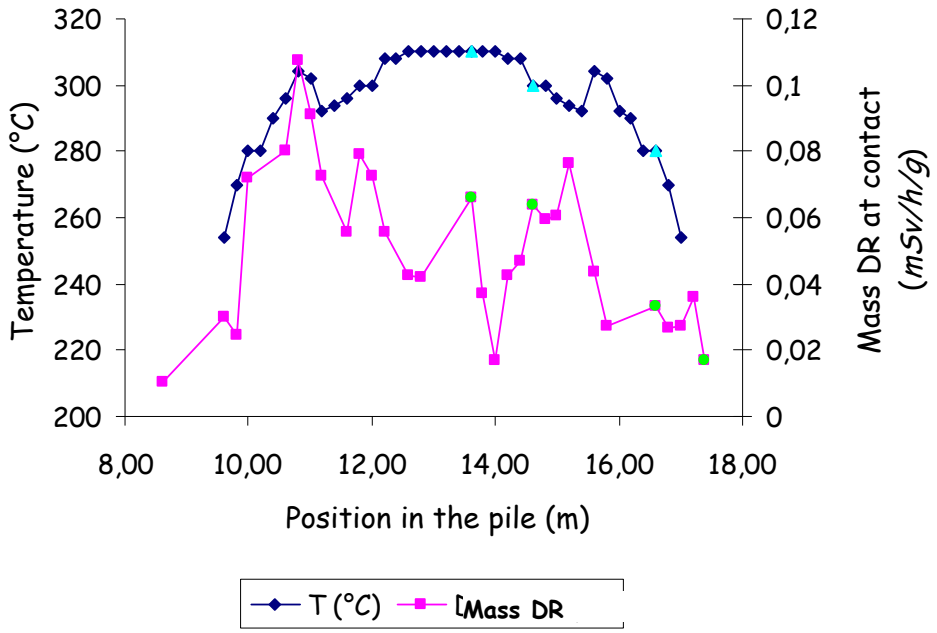


FIGURE 7: PROFILE OF GRAPHITE TEMPERATURE DURING THE OPERATION OF THE REACTOR AND OF THE MASS DOSE RATE AT CONTACT WITH VERTICAL-CORING GRAPHITE SAMPLES IN RELATION TO THE POSITION OF THE CORES IN THE PILE

It is possible to note that the difference between the operating temperature and the dose rate of the moderator samples is only slight. The reflector sample has very different characteristics (lower dose rate and temperature, different fabrication). Since the collected cores in the G2 reactor measure 20 cm in length and 3 cm in diameter, it is necessary to cut them for the leaching tests and characterisations. The diagrams displayed in Figure 8 and Figure 9 show the cuts made on the cores from the graphite moderator and reflector of the G2 reactor.

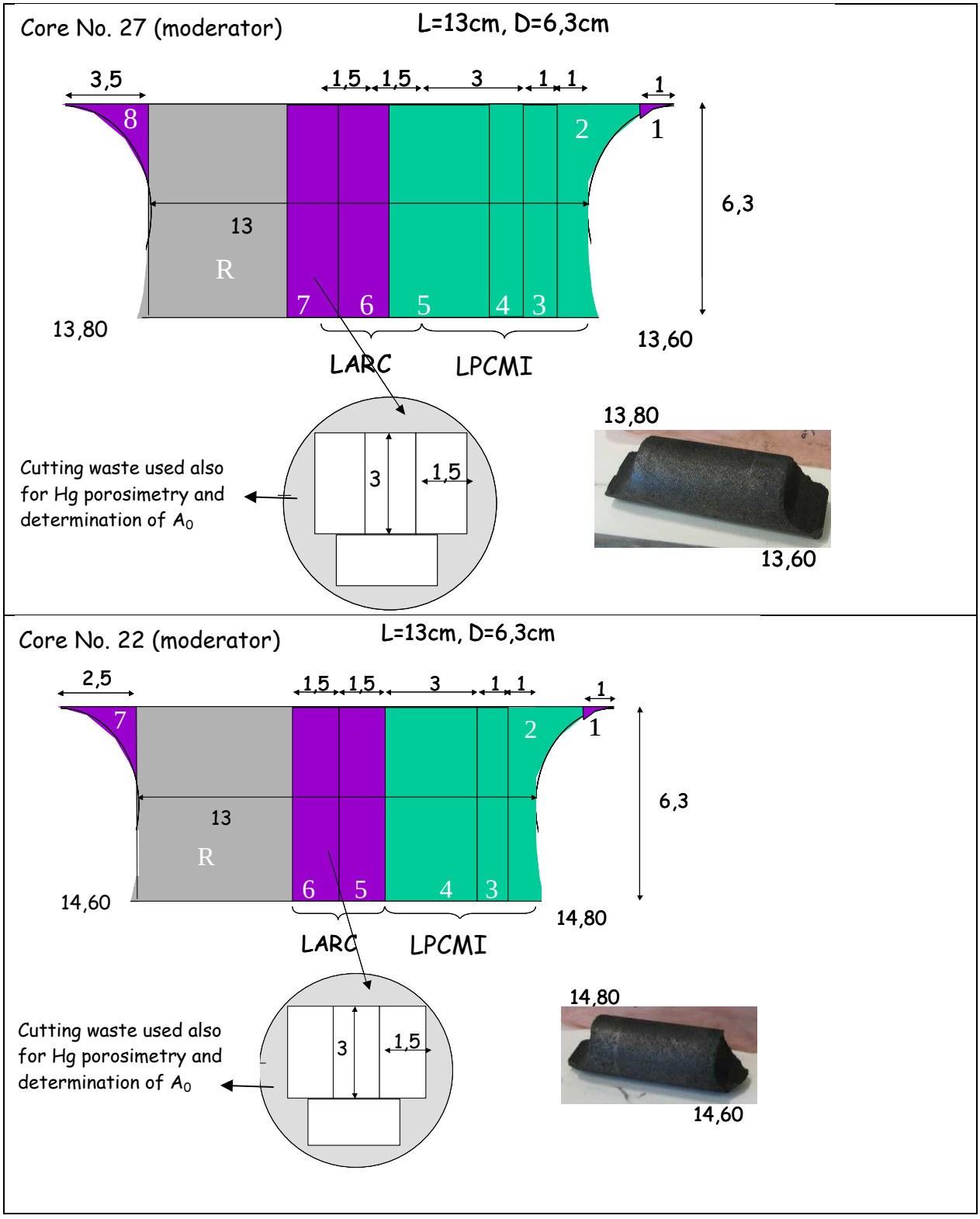


FIGURE 8: CUTS MADE ON CORES NOS. 27 AND 32 OF THE G2 GRAPHITE MODERATOR

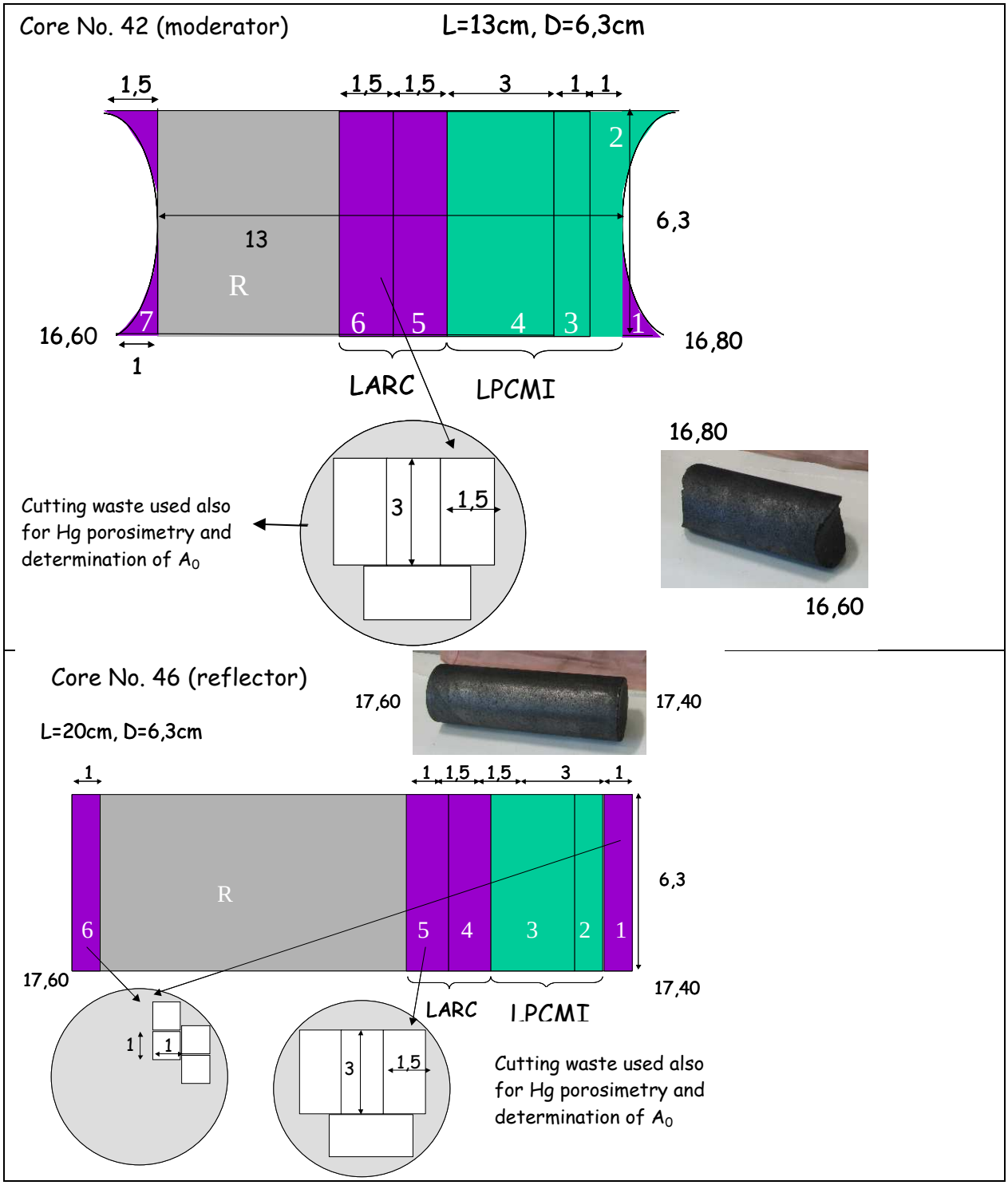


FIGURE 9: CUTS MADE ON CORES NOS. 42 AND 46 OF THE G2 GRAPHITE MODERATOR AND REFLECTOR

The two central lamellae are designed for leaching and impregnation tests with density measurements. The cutting waste from the central lamella and the pieces collected at the extremities are intended for various characterisation purposes: density, mercury porosimetry, helium pycnometry and determination of the initial $^{36}Cl$ activity. Intermediate lamellae were cut for LPCMI geometric and hydrostatic densities, X-ray diffraction and Raman spectroscopy measurements.

The overall information is displayed in Table 7.

| Sample | Lamella | Laboratory | Geometric density | Mercury porosity | Helium pycnometry | Bromo-benzene | DRX | Leach | $^{36}Cl$ | SIMS |
|---|---|---|---|---|---|---|---|---|---|---|
| G2-27 13.60-13.80 | 1 | LARC/LECD | | X | X | | | | x | |
| | 2 | SEMI | | | | | | | | |
| | 3 | SEMI | X | | | x#1 | x#1 | | | |
| | 4 | SEMI | X | | | | | | | |
| | 5 | SEMI | X | | | | | | | |
| | 6 | LARC | X | | | | | X | | |
| | 7 | LARC/LECD | X#1 | x#1 | x#1 | | | x#1 | x#1 | x#1 |
| | 8 | LARC/LECD | | x | x | | | | x | |
| | Reserve | LARC | | | | | | | | |
| G2-32 14.60-14.80 | 1 | LARC/LECD | | x | x | | | | x | |
| | 2 | SEMI | x | | | | | | | |
| | 3 | SEMI | x | | | x#1 | x#1 | | | |
| | 4 | SEMI | x | | | | | | | |
| | 5 | LARC/LECD | x | | | | | x | | |
| | 6 | LARC/LECD | x#1 | x#1 | x#1 | | | x#1 | x#1 | x#1 |
| | 7 | LARC/LECD | | x | x | | | | x | |
| | Reserve | LARC | | | | | | | | |
| G2-42 16.60-16.80 | 1 | LARC/LECD | | x | x | | | | x | |
| | 2 | SEMI | | | | | | | | |
| | 3 | SEMI | x | | | X | x#1 | | | |
| | 4 | SEMI | x | | | | | | | |
| | 5 | LARC | x | | | | | x | | |
| | 6 | LARC/LECD | | x#1 | x#1 | | | x | x | x#1 |
| | 7 | LARC/LECD | | x#1 | x#1 | | | | x | |
| | Reserve | LARC | | | | | | | | |
| G2-46 17.40-17.60 | 1 | LARC/LECD | | x | X | | | | x | |
| | 2 | SEMI | x | | | x | x#1 | | | |
| | 3 | SEMI | x | | | | | | | |
| | 4 | LARC | x | | | | | | x | |
| | 5 | LARC/LECD | x#1 | x#1 | x#1 | | | x | x | x#1 |
| | 6 | LARC/LECD | | x#1 | x#1 | | | | x | |
| | Reserve | LARC | | | | | | | | |

TABLE 7: SUMMARY TABLE OF THE USES FOR SAMPLES

*#1 Measurement taken on a subsample of the initial lamella.*

# 5 Graphite characterisation

In order to understand the radionuclide-release phenomenon during graphite-leaching tests and to study the evolution of its microstructure, it is necessary to characterise the initial samples. In order to achieve that goal, various geometric-density and hydrostatic measurements with bromobenzene, helium pycnometry and mercury porosimetry were made, together with characterisations by X-ray diffraction and Raman spectroscopy, on active and inactive samples of the G2 reactor. Those measurements were made at the LARC in co-operation with the LECD of CEA CADARACHE, and at the LPCMI of CEA SACLAY.

## *5.1. Density measurements*

Geometric densities are obtained by:

- measuring the dimensions of the samples with a sliding calliper (uncertainty of 0.1 mm) by recording several readings per level, and
- weighing samples on precision scales.

The propagation of uncertainties, notably on average values was calculated in accordance with engineering techniques (Ref. R280).

## *5.2. Helium pycnometry*

The non-destructive technique known as pycnometry by helium displacement is used to measure the internal volume of a porous material and to deduce its density from its mass. The measurement principle relies on the properties of helium, which behaves like a pure gas. It is first pressurised within a reference chamber of a known volume before opening the pressurised chamber (sample) of a known volume. Pressure changes are associated with the porosity of the sample. Gas fills up the open porosities of the sample, while only the dense fraction and the sealed porosities of the sample remain inaccessible. The cells being used allow for measurements to be taken on samples in an order ranging from 1 to 10 g more or less.

## 5.3. Mercury porosimetry

The destructive technique known as porosimetry by mercury intrusion is designed to determine the distribution of the pore sizes within a porous material, whether solid or powdery. The measurement principle relies on the properties of a non-wetting liquid at ambient temperature, such as mercury. In order to penetrate into the pores of a porous material, mercury needs to be forced in. Any intrusion pressure, $P$, which is necessary for mercury to penetrate in a pore with a diameter, $d$, is provided by the Laplace relation, as follows :

$$P = \frac{4\gamma \cos\theta}{d} \qquad (1)$$

where $P$ is the intrusion pressure of mercury ($Pa$)

$\gamma$ is the surface tension of mercury ($Pa/m$)

$\theta$ is the wetting angle of mercury on pore surface (°)

$d$ is the pore diameter

The pressure applied to mercury is raised by increments and the mercury volumes penetrating in the porous solid are recorded at every increment. The end result is the cumulated porous volume in relation to intrusion pressure and, consequently, to pore diameter. The derivative provides the porous distribution of the solid.

However, that study method includes some constraints, such as :

- more particularly, the high pressure (in the order of 400 MPa) being applied to mercury for penetrating into the finest pores (measuring a few nanometres in diameter) may modify or destroy the porous network of the material under study. The mechanical strength to the compression of the graphite is approximately 25 MPa and corresponds to entrance pore diameters in the order of 50 nm. Beyond half that pressure, which corresponds to a diameter of 100 nm, it is recognised that measurements cease to be representative of the material, whose porous network may be modified (opening/creation of porosity),

- referring to Laplace's Law is equal to assimilating all pores to cylinders, which is very far from being realistic. In addition, it is important to remember that we are only being sensitive to the entrance diameter of the pores. In fact, significant hysteresis phenomena may hide the reality of the porous structure, as in the case of bottle-shaped pores, which may contain a large quantity of mercury, in spite of their very small entrance diameter,
- the pores being reached do not allow to cover the entire porosity range of the samples. Helium as a gas and with its atomic diameter (2.3 Å [15] [7]), which is much smaller than that of mercury, is more suitable for probing correctly the open porosity of graphite.

However, the major interest of that technique is to represent the distribution of pore sizes and to compare various types of graphite by proposing a conventional display of the porous structure.

During this study, two *Micromeritics* porosimeters (Model 9420) were used: one for measuring inactive samples and the other, being placed in a glove box, to record measurements in a radioactive environment.

## *5.4. Bromobenzene hydrostatic density*

The measurement principle for the hydrostatic density of a body is based on Archimedes' principle. It consists in a double weighing, the first being conducted in air, and the second in bromobenzene.

The actual mass (Ma) of a sample is equal to its apparent mass, to which buoyancy must be added. Both weighings, in air and in bromobenzene, respectively, provide the following equation :

$$Mr = M_1 + (Ve.\ \rho_a) = M_2 + (Ve.\ \rho_b) \quad (2)$$

where :

*Mr* is the effective mass of the sample
$M_1$ is the mass of sample weighed in air
$M_2$ is the mass of the sample weighed in bromobenzene
$\rho_a$ is the air density
$\rho_b$ is the bromobenzene density
*Ve* is the geometric volume of the sample. In that case, the sample is weighed in bromobenzene, but the bromobenzene does not wet the sample

It is therefore possible to calculate the geometric volume (*Ve*) of the sample through relation (3), as follows:

$$Ve = \frac{M_1 - M_2}{\rho_b - \rho_a} \quad (3)$$

from which it is therefore possible to deduce the geometric density of the sample ($\rho_g$), as follows :

$$\rho_g = \left[\frac{M_1\left[\rho_b - \rho_a\right]}{M_1 - M_2}\right] + \rho_a \quad (4)$$

If bromobenzene is submitted to a vacuum before immersing the sample into it for weighing purposes, it will imbibe all open pores of the sample (Figure 10), thus allowing a mass, $M_3$, which is the mass of the sample as weighed in bromobenzene after imbibition to be determined.

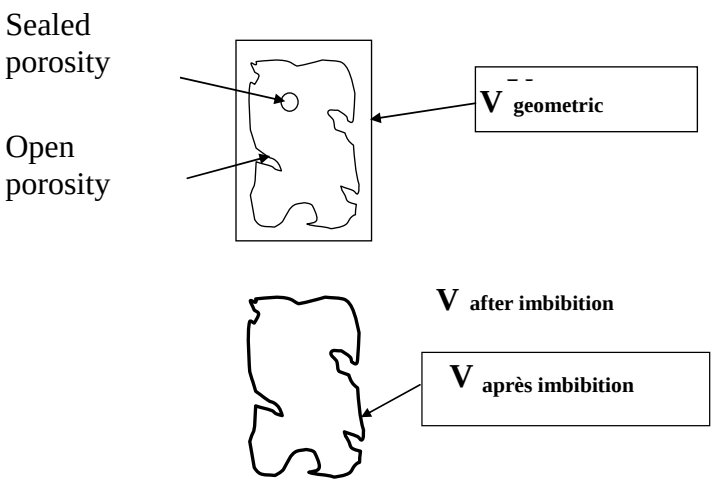


FIGURE 10: GEOMETRIC VOLUME ($V_e$) AND VOLUME AFTER IMBIBITION ($V_e$-$V_{p0}$)

Both weighings in bromobenzene, before and after imbibition, provide the following equation (5) :

$$Mr = M_2 + (Ve.\ \rho_b) = M_3 + (Ve - Vpo)\ \rho_b \qquad (5)$$

where *Vpo* is the volume of open porosity.

Hence, it is possible to calculate the volume of the open porosity (*Vpo*) of the sample by relation (6) :

$$Vpo = \frac{M_3 - M_2}{\rho_b} \qquad (6)$$

and deduce the pycnometric density ($\rho_p$) of the sample, as follows :

$$\rho_p = \frac{Mr}{V_e - Vpo}$$

$$\rho_p = \left[ \frac{M_3 [\rho_b - \rho_a] \rho_b}{[M_1 - M_3] \rho_b + [M_3 - M_2] \rho_a} \right] + \rho_b \qquad (7)$$

## 5.5. Expression of results

Pore-distribution calculations (total porosity, open and sealed porosities) were made in accordance with the following relations :

The total porosity ($P_T$) is :

$$P_T(\%) = 100\left(1 - \frac{\rho_G}{\rho_{th}}\right) \quad (8)$$

where $\rho_{th}$ is the theoretical density of graphite crystal (2.266) and $\rho_G$ is its measured geometric density.

The open porosity ($P_O$) is :

$$P_O(\%) = 100\left(1 - \frac{\rho_G}{\rho_S}\right) \quad (9)$$

where $\rho_S$ is the density of the skeleton, as measured by helium pycnometry or by hydrostatic measurement in bromobenzene.

The sealed porosity ($P_S$), which is inaccessible to helium, is :

$$P_F = P_T - P_O \quad (10)$$

## 5.6. X-ray diffraction

A Siemens D500 ‘θ/2θ’ diffractometer with a copper anticathode (Cu Kα1 and Cu Kα2 radiation) is used and set into a shielded cell (Figure 11). In order to collimate the X-ray beam, the device is equipped with slits before and after the sample in accordance with the following optical scheme: 1° slit/ 0.3° slit/ sample/0.3° slit/Soller slits/0.05° slit. Furthermore, in order to filter potential stray radiation, the device is equipped with a back graphite monochromator (filtering of $K_\beta$ radiation of copper and of stray X and γ radiation).

Acquisitions consisted in phase recordings in 'θ/2θ' mode (variable impact) over a range varying between 20 and 90° 2θ. Diffractograms were recorded at 40 kV/30 mA (X-ray generator), with a pitch of 0.02° and a counting time of 10 s per pitch.

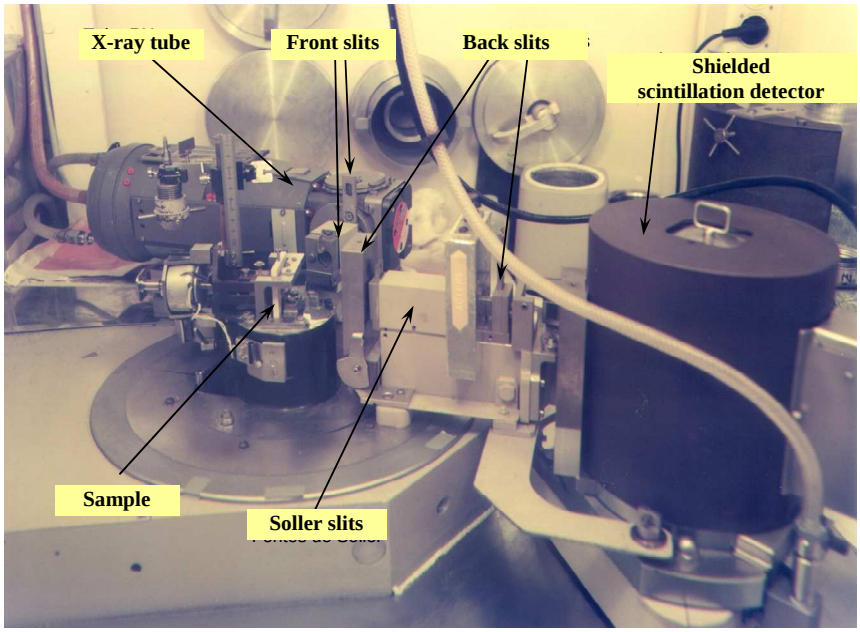


FIGURE 11: X-ray DIFFRACTOMETER IN SHIELDED CELL (LPCMI)

## 5.7. Raman spectroscopy

A Jobin-Yvon T64000 triple-analysis-network Raman spectrometer, using a 2 W argon laser (λ = 514 nm) and coupled with an optical microscope designed to enlarge up to one hundred fold (optical observation of the sample and focusing of the laser on the analysis zone). The spectrometer and the laser are coupled with two analysis stations, one "cold" for studying non-irradiated materials, and the other in a shielded cell for characterising activated samples (Figure 12). For the "cold" station (BX40 microscope), the laser/microscope/spectrometer connection is made through an optical path with mirrors. For the shielded-cell station, the connection between the laser exciter, the sample positioned under a nuclearised microscope (BX50) in Cell M16,and the spectrometer is made with optical fibres.

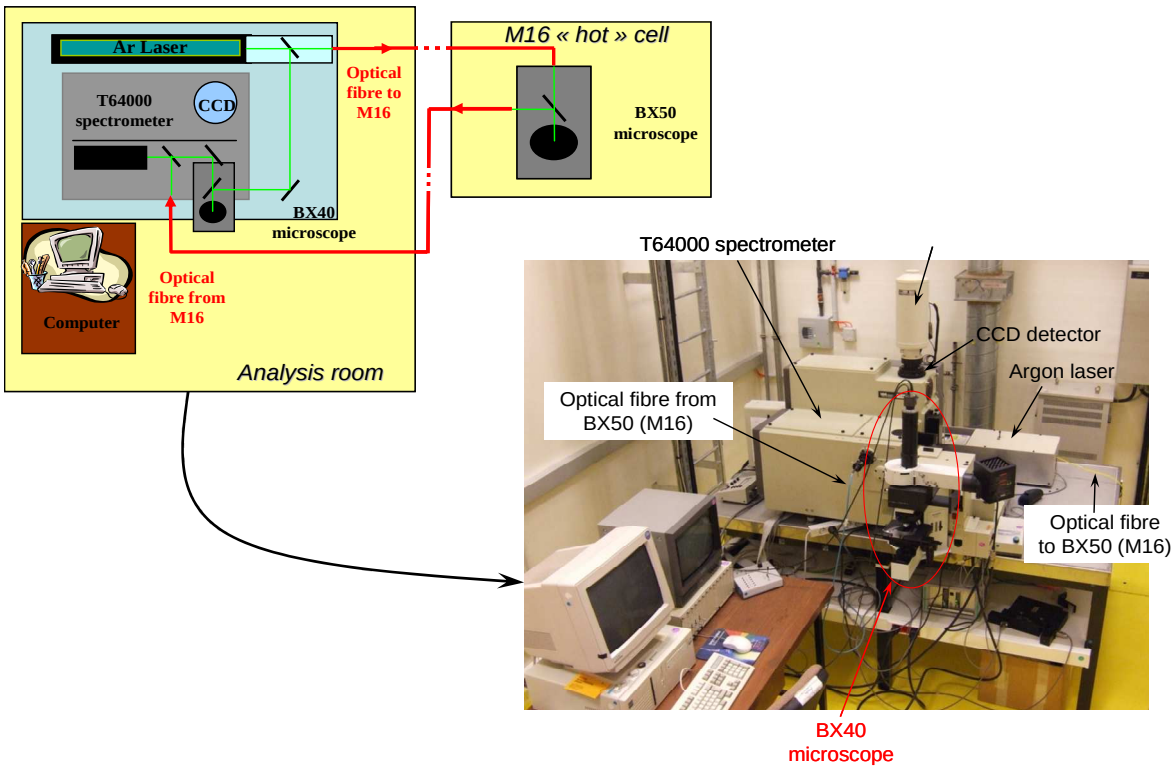


FIGURE 12: RAMAN-SPECTROMETRY INSTALLATION (LPCMI)

For technical reasons (connection problem between the nuclearised microscope and the optical fibre linked to the spectrometer) the Raman characterisation of the G2 graphite has not been performed yet on samples X1-1, Y3-2 and Z1-1 in line with the following experimental conditions:

– laser power: 200 mW at laser output
– acquisition windows: between 1,250 and 1,800 $cm^{-1}$
– counting time: 1 background count + 2 acquisition counts (3 × 120 s)
– microscope lens: × 100

# 6 Results from G2 virgin graphite samples

## 6.1. Geometric-density measurements

Density measurements were made on a lamella of virgin graphite brick from the G2 reactor. Since that graphite block is machined (tracks of fuel channels), it should be noted that it is possible to deduce that it consists of core-graphite remains. That graphite must have been developed from "Special" Grade-A coke and its apparent theoretical density is 1.71. The LARC and the LPCMI worked on lamellae Nos. 4 and 1, respectively. For the time being, no inactive graphite sample is available from the reflector.

### 6.1.1. Density on samples collected at the core of the brick

Small samples, which are used for preliminary water-impregnation tests, were measured in order to determine their geometric densities. They include prismatic samples measuring between 1 and 1.5 cm square by 1 to 3 cm in length. Those samples, which were used for leaching tests, come from the core subsample of lamella No. 4 and identified as No. 5 on the cutting plan.

| Subitem of lamella No. 4 | Mass (*g*) | Average size (*cm*) | $\rho_G$ |
|---|---|---|---|
| **5-1** | 7.2085 | 1.97*1.51*1.48 | 1.63±0.05 |
| **5-2** | 3.6199 | 1.51*1.46*1.02 | 1.61±0.04 |
| **5-3** | 10.4770 | 1.48*1.4*2.89 | 1.66±0.06 |
| **5-4** | 1.7116 | 1.02*1.00*0.97 | 1.73±0.06 |
| **5-5** | 4.7425 | 1.02*1.00*2.88 | 1.63±0.06 |
| **5-6** | 4.3433 | 1.02*0.99 *2.87 | 1.64±0.05 |
| **5-7** | 4.8074 | 1.02*1.00*2.88 | 1.67±0.06 |
| **5-8** | 10.9432 | 1.51*1.51*2.89 | 1.66±0.03 |
| **5-9** | 11.9068 | 2.88*0.74*3.00 | 1.63±0.05 |
| **5-10** | 15.526 | 3.01*1.07*2.88 | 1.68±0.04 |
| **5-11** | 10.7028 | 2.84*1.48*1.51 | 1.68±0.06 |
| **Average** | | | **1.66 ± 0.07** |
| **Minimum** | | | **1.61 ± 0.04** |
| **Maximum** | | | **1.73 ± 0.06** |

TABLE 8: GEOMETRIC-DENSITY MEASUREMENTS MADE ON G2 VIRGIN GRAPHITE – CASE OF SAMPLES USED FOR LEACHING TESTS AND COLLECTED FROM THE BRICK CORE OF LAMELLA NO. 4

It was observed that the values are rather dispersed – ranging from 1.61 to 1.73 – and that the average density of such small samples is 1.66, whereas the expected density would be 1.71.

Following the first results, larger samples were cut at the LARC from the same lamella of the G2 brick, which was recut from the items collected from the core part of the brick (under items No. 5).

| Type | Piece no. | Mass (*g*) | Average size (*cm*) | $\rho_G$ |
|---|---|---|---|---|
| **Core** | 5-12 | 43.4214 | 3.02*2.87*3.02 | 1.66±0.02 |
| **Core** | 5-13 | 44.1425 | 3.02*2.89*3.03 | 1.67±0.02 |
| **Core** | 5-14 | 43.6621 | 3.00*2.88*3.01 | 1.68±0.02 |
| **Core** | 5-15 | 15.1900 | 2.88*1.06*3.01 | 1.66±0.04 |
| **Core** | 5-16 | 18.6911 | 1.98*1.97*2.87 | 1.67±0.03 |
| **Core** | 5-17 | 18.6582 | 1.99*1.97*2.88 | 1.65±0.03 |
| **Average** | | | | **1.67±0.03** |
| **Minimum** | | | | **1.65±0.03** |
| **Maximum** | | | | **1.68±0.02** |

TABLE 9: GEOMETRIC-DENSITY MEASUREMENTS MADE AT LARC ON G2 VIRGIN GRAPHITE – CASE OF SAMPLES CUT FROM THE BRICK CORE

It was observed that, on average, the new series of measurements on brick-core subsamples may be grouped, apart from measurement uncertainties, with the first series (density of 1.67±0.02), with due account of a lesser dispersion of values from 1.65 to 1.68. Such reduction in dispersion is probably due to the fact that the samples are larger in volume. However, the measured density is still lower than the generally acknowledged one for samples consisting of "Special" Grade-A based graphite.

Slightly lower values were obtained at the LPCMI on 14 samples collected from the core of lamella No. 1, whose dimensions (ϕ 20 mm / h 20 mm) are close to those of the samples characterised at the LARC (see Figure 5 for the LPCMI sampling plan). The measurements presented in Table 10 show that the average density, as measured in the brick core, is 1.59 with a dispersion range between 1.50 and 1.65.

| Sample reference | Sample no. | Diameter (*cm*) | Length (*cm*) | Mass (*g*) | Volume ($cm^3$) | Density |
|---|---|---|---|---|---|---|
| Y | 5.1 | 1.996 | 2.028 | 10.478 | 6.343 | 1.652 |
| | 5.2 | 1.999 | 1.957 | 10.105 | 6.140 | 1.646 |
| | 6.1 | 1.999 | 1.994 | 10.106 | 6.260 | 1.614 |
| | 6.2 | 1.993 | 1.987 | 9.915 | 6.201 | 1.599 |
| | 7.1 | 0.997 | 0.894 | 1.061 | 0.698 | 1.520 |
| | 7.2 | 1.001 | 2.003 | 2.439 | 1.575 | 1.549 |
| | 8.1 | 1.000 | 0.985 | 1.162 | 0.774 | 1.502 |
| | 8.2 | 0.997 | 1.821 | 2.183 | 1.422 | 1.535 |
| X | 2.1 | 1.999 | 0.799 | 4.102 | 2.505 | 1.637 |
| | 2.2 | 1.998 | 0.901 | 4.517 | 2.825 | 1.599 |
| | 2.3 | 1.982 | 0.821 | 4.104 | 2.535 | 1.619 |
| Y | 2.1 | 1.999 | 0.836 | 4.258 | 2.624 | 1.623 |
| | 2.2 | 1.996 | 0.905 | 4.491 | 2.830 | 1.587 |
| | 2.3 | 1.991 | 0.773 | 3.899 | 2.405 | 1.621 |
| **Average** | | | | | | **1.59±0.05** |
| **Minimum** | | | | | | **1.50** |
| **Maximum** | | | | | | **1.65** |

TABLE 10: GEOMETRIC-DENSITY MEASUREMENTS MADE ON G2 VIRGIN GRAPHITE – CASE OF SAMPLES COLLECTED AT THE CORE OF THE BRICK OF LAMELLA NO. 1

Those measurements were completed by others at the edge of the brick.

### 6.1.2 Density on the samples collected at the edge of the brick

Edge samples resulting from the cutting of lamella No. 4 were measured and weighed (see cutting plan) with a view to providing density values at the edge of the brick.

| Type | Item no. | Mass (*g*) | Average size (*cm*) | $\rho_G$ |
|---|---|---|---|---|
| **Edge** | 1 | 57.2185 | 3.01*2.86*3.89 | 1.71±0.02 |
| **Edge** | 2 | 58.3973 | 3.01*2.88*3.83 | 1.76±0.02 |
| **Edge** | 3 | 56.8173 | 3.03*2.86*3.79 | 1.73±0.02 |
| **Edge** | 4 | 58.7388 | 3.01*2.88*3.93 | 1.72±0.02 |
| **Edge** | 6 | 148.1919 | 3.01*2.89*9.95 | 1.71±0.03 |
| **Edge** | 7 | 88.6698 | 2.88*1.77*10.07 | 1.73±0.07 |
| **Edge** | 8 | 86.2461 | 2.88*1.75*9.95 | 1.72±0.06 |
| **Edge** | 9 | 149.6542 | 3.02*2.89*10.01 | 1.71±0.02 |
| **Average** | | | | **1.72±0.05** |
| **Minimum** | | | | **1.71±0.02** |
| **Maximum** | | | | **1.76±0.02** |

TABLE 11: GEOMETRIC-DENSITY MEASUREMENTS MADE ON G2 VIRGIN GRAPHITE – CASE OF CUT SAMPLES AT THE EDGE OF LAMELLA NO. 4

It was observed that the measurements made on samples from the edge of lamella No. 4 show an average density of 1.72 ± 0.03 with a dispersion range between 1.71 and 1.76. Consequently, it was also observed that the density of the G2 block is heterogeneous between the inside and the outside of the brick, which may be explained by a lesser impregnation of the brick core.

Those measurements were completed by others at the edge of lamella No. 1 on 20 samples (see cutting plan, Figure 5).

| Sample reference | Sample no. | Diameter (*cm*) | Length (*cm*) | Mass (*g*) | Volume ($cm^3$) | Density |
|---|---|---|---|---|---|---|
| **Y** | 1 | 2.006 | 1.999 | 10.588 | 6.319 | 1.676 |
| | 2 | 2.001 | 1.987 | 10.486 | 6.246 | 1.679 |
| | 3.1 | 1.998 | 2.002 | 10.500 | 6.276 | 1.673 |
| | 3.2 | 1.995 | 0.795 | 4.021 | 2.484 | 1.619 |
| | 4.1 | 1.998 | 1.985 | 10.278 | 6.222 | 1.652 |
| | 4.2 | 1.986 | 1.937 | 9.741 | 6.002 | 1.623 |
| | 9.1 | 1.002 | 0.902 | 1.157 | 0.712 | 1.625 |
| | 9.2 | 0.999 | 2.164 | 2.701 | 1.696 | 1.592 |
| | 10.1 | 1.002 | 0.899 | 1.162 | 0.708 | 1.641 |
| | 10.2 | 1.000 | 2.051 | 2.640 | 1.611 | 1.639 |
| | 11.1 | 0.998 | 2.002 | 2.446 | 1.564 | 1.564 |
| | 11.2 | 1.001 | 2.002 | 2.546 | 1.575 | 1.616 |
| | 12.1 | 1.000 | 2.004 | 2.554 | 1.574 | 1.622 |
| | 12.2 | 0.999 | 2.009 | 2.538 | 1.575 | 1.611 |
| **X** | 1.1 | 2.001 | 0.835 | 4.425 | 2.624 | 1.686 |
| | 1.2 | 1.998 | 0.902 | 4.727 | 2.827 | 1.672 |
| | 1.3 | 1.991 | 0.859 | 4.538 | 2.674 | 1.697 |
| **Z** | 1.1 | 1.986 | 0.900 | 4.752 | 2.788 | 1.705 |
| | 1.2 | 1.987 | 0.717 | 3.795 | 2.225 | 1.706 |
| | 1.3 | 1.986 | 0.829 | 4.394 | 2.569 | 1.710 |
| **Average** | | | | | | **1.65±0.04** |
| **Minimum** | | | | | | **1.56** |
| **Maximum** | | | | | | **1.71** |

TABLE 12: GEOMETRIC-DENSITY MEASUREMENTS MADE ON G2 VIRGIN GRAPHITE – CASE OF CUT SAMPLES AT THE EDGE OF LAMELLA NO. 1

Those measurements also show a density gradient between the samples collected at the edge and at the core of the brick. The resulting measurements show that the average density at the edge is 1.65 with a dispersion range between 1.56 and 1.71.

### 6.1.3 Density on large sample

With due account of the differences that were observed at the various sampling scales and zones involved and in order to determine whether the characterised brick is truly representative of the G2 pile, it was decided to perform a measurement on the remaining block, which is larger in both size and mass, with a view to providing an average value that would involve all density gradients. Average rates are displayed in Table 13.

**Measurement of half-cylinders**

| | Length 1 | Length 2 |
|---|---|---|
| Cylinder A | 3,48 | 6,99 |
| | 3.43 | 7.01 |
| | | 7.04 |
| Average | 3.46 | 7.01 |
| Stand. dev. | 0.03 | 0.03 |
| Delta | 0.03 | 0.03 |
| Cylinder B | 3.51 | 7.10 |
| | 3.44 | 7.08 |
| | | 7.05 |
| Average | 3.48 | 7.08 |
| Stand. dev. | 0.05 | 0.03 |
| Delta | 0.05 | 0.03 |

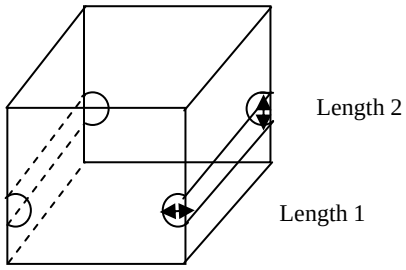


**Measurement of face levels**

| | Length cm | Width (*cm*) | Height (*cm*) |
|---|---|---|---|
| Face 1 | 23,00 | 20,00 | |
| | 22,94 | 20,00 | |
| | 22,90 | 20,00 | |
| Face 2 | 22,90 | 20,00 | |
| | 22,91 | 20,01 | |
| | 22,94 | 20,00 | |
| Face 3 | 22,93 | | 20,00 |
| | 22,90 | | 20,00 |
| | 22,91 | | 20,00 |
| Face 4 | 22,98 | | 20,01 |
| | 22,96 | | 20,01 |
| | 22,94 | | 20,01 |
| Face 5 | | 20,00 | 20,00 |
| | | 20,00 | 20,00 |
| | | 19,99 | 20,00 |
| Face 6 | | 19,99 | 20,00 |
| | | 20,00 | 20,00 |
| | | 20,00 | 20,00 |
| Average | 22,93 | 20,00 | 20,00 |
| Stand. dev. | 0,03 | 0,01 | 0,00 |
| Delta | 0,03 | 0,01 | 0,01 |

TABLE 13: DENSITY OF THE G2 VIRGIN BLOCK SAMPLE

In the end, we obtain a volume block measuring 8,295 ± 20 $cm^3$ with a mass of 14,240 ± 10 g i.e., a sample with a geometric density of 1.717±0,009, which is close to the values recorded in the literature and also obtained on larger samples.

### 6.1.4 Summary of geometric-density measurements

For the entire set of characterised samples, measurements highlighted a density gradient between the less dense core of the brick and the edge, with an average difference of 0.05. That radial gradient should be attributed to the impregnation of G2 bricks, which is less comprehensive at the core of the brick. In addition, if the low density values recorded at first on small samples may have raised a doubt with regard to the exact nature of the characterised graphite, further measurements on the whole block confirmed that the brick being used as non-irradiated reference material was actually G2 graphite with a density of 1.717.

Table 14 summarises the measurements that were made.

| | **Measurem.[1] lamella No. 4** | **Measurem.[2] lamella No. 4** | **Measurem. lamella No. 4** | **Measurem. Block** | **Measurem. lamella No. 1** | **Measurem. lamella No. 1** |
|---|---|---|---|---|---|---|
| **Sampling** | **Core** | **Core** | **Edge** | **Block** | **Core** | **Edge** |
| **Average** | 1.66±0.07 | 1.67±0.03 | 1.72±0.05 | 1.717±0.009 | 1.59±0.05 | 1.65±0.04 |
| **Minimum** | 1.61±0.04 | 1.65±0.03 | 1.71±0.02 | – | 1.50 | 1.56 |
| **Maximum** | 1.73±0.06 | 1.68±0.02 | 1.76±0.02 | – | 1.65 | 1.71 |
| **Number** | 11 | 6 | 8 | 1 | 14 | 20 |
| **Total porosity %** | 26.9±1.2 | 26.5±0.5 | 23.9±0.7 | 24.2±0.1 | 29.8±0.9 | 27.2±0.7 |

TABLE 14: SUMMARY OF GEOMETRIC-DENSITY MEASUREMENTS

[1] *Case of samples used for impregnation tests.* [2] *Other samples.*

It is possible to note that, on average, lamella No. 1 is less dense that lamella No. 4, and consequently, that the total porosity is higher. With due account of the fact that the brick results from the cutting of a whole brick, it is not possible to conclude that lamella No. 1 is at the edge of the brick. Lamella No. 4, whose densities are closer to that of the block, may be considered as more representative of the reference material.

## 6.2. Helium pycnometry

A helium-pycnometry measurement was taken on a G2 virgin graphite sample from the brick core of lamella No. 4. A density of 2.15±0.05 was deduced for the G2 skeleton. Identical measurements were made at the LPCMI on samples collected from the core (Y7.1 and Y8.1) and at the edge (Y9.1 and Y10.1) of lamella No. 1. Both samples provided an identical density value of 2.17 for the G2 skeleton. Value results are displayed in Table 15.

| Lamella | Sample no. | Sample position | Average density ($\rho_G$) | Total porosity (%) | Helium pycnometry density ($\rho_S$) | Open porosity (%) | Sealed porosity (%) |
|---|---|---|---|---|---|---|---|
| 1 | Y7.1 | Core | 1.520 | 32.92 | 2.173 | 30.05 | 2.87 |
| | Y8.1 | Core | 1.502 | 33.72 | 2.169 | 30.75 | 2.96 |
| | Y9.1 | Edge | 1.625 | 28.29 | 2.168 | 25.05 | 3.24 |
| | Y10.1 | Edge | 1.641 | 27.58 | 2.170 | 24.38 | 3.20 |
| 4 | 5 | Core | 1.69 | 25.6±0.9 | 2.15±0.05 | 21.7±1.2 | 3.9±1.5 |

TABLE 15: HELIUM-PYCNOMETRY MEASUREMENTS

Measurements show that the density gradient between the brick core and edge is reflected essentially by a higher open porosity in the brick core, while the sealed porosity does not vary.

Figure 13 illustrates the correlation between open porosity and the density of samples. As density increases, the open porosity decreases, thus demonstrating that impregnation has reduced part of the open porosity of the graphite. That result confirms the bibliographical data[7].

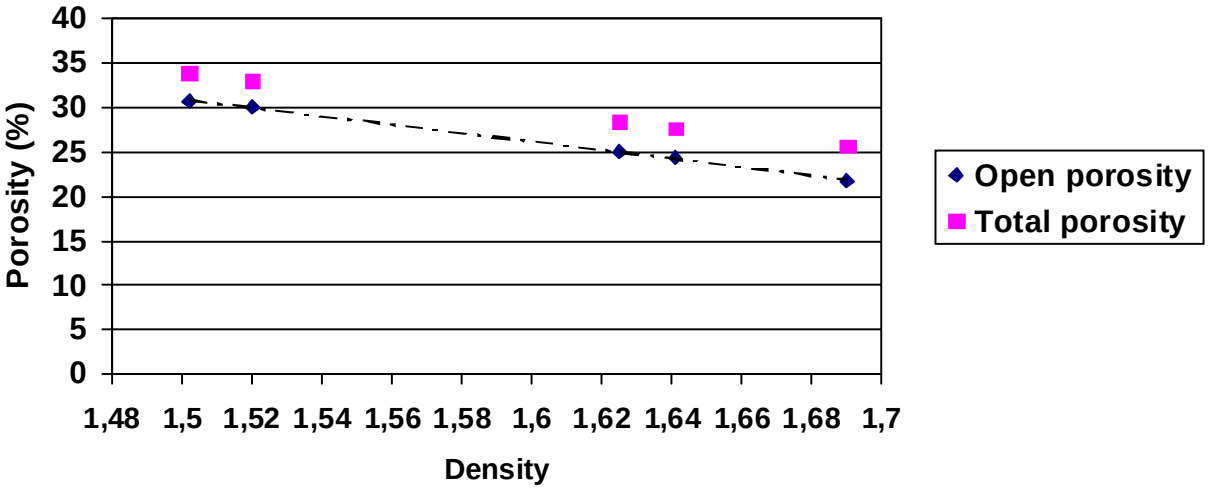


FIGURE 13: CORRELATION BETWEEN DENSITY AND OPEN POROSITY OF THE SAMPLES

## 6.3. Mercury porosimetry

The results from mercury measurements taken with an inactive porosimeter on five inactive graphite samples are shown on the following figures. Figure 14 and Figure 15 show the evolution of the cumulated porous volume in relation to pore diameter and the distribution of pore diameters, respectively. It was observed that a large part of the total porous volume of the sample lies within a pore-diameter range between 1 and 30 µm. A second peak was also noted, but on a very broad range of pore sizes, thus confirming a primarily a macroporous solid.

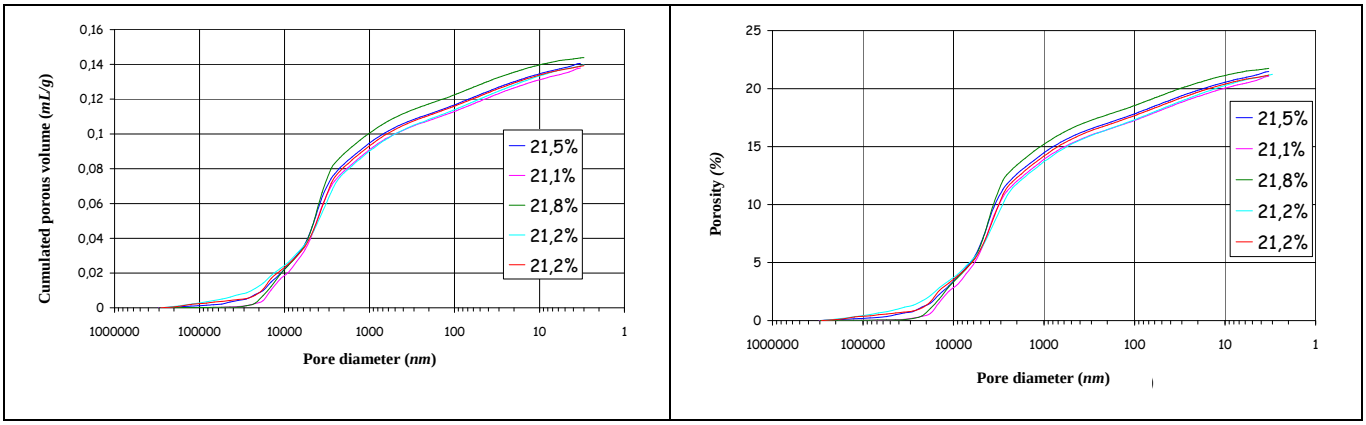


FIGURE 14: EVOLUTION OF CUMULATED POROUS VOLUME IN ML/G AND IN % IN RELATION TO THE PORE DIAMETER FOR FIVE G2 VIRGIN GRAPHITE SAMPLES

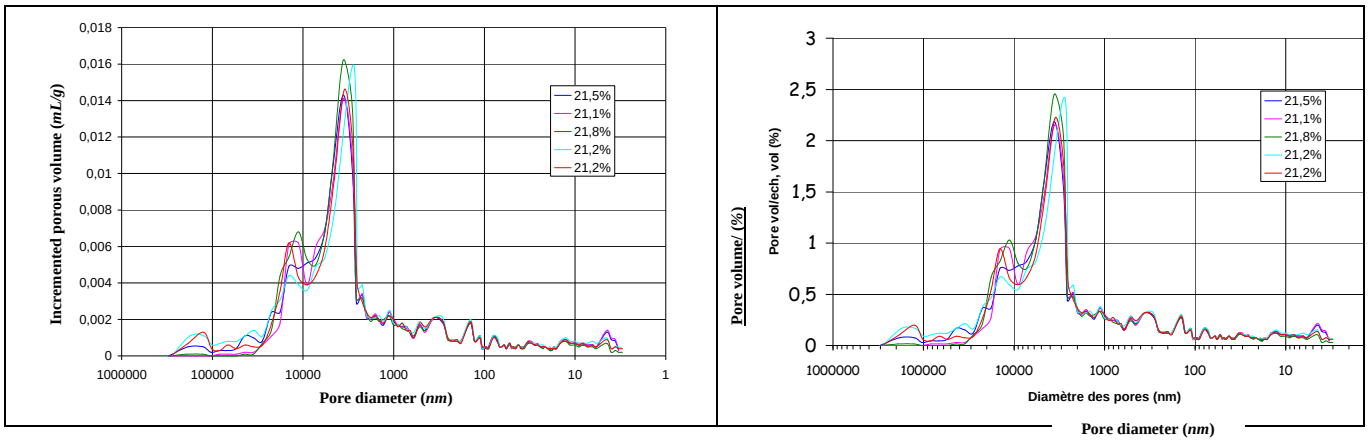


FIGURE 15: PORE-DIAMETER DISTRIBUTION IN ML/G AND IN % IN RELATION TO THE POROUS VOLUME OF THE SAMPLE AS MEASURED FOR FIVE G2 VIRGIN GRAPHITE SAMPLES

Those figures illustrate the sound reproducibility of the five analyses on G2 virgin graphite, which is reflected by the low dispersion rates being measured on the main parameters.

| Sample | Test 1 | Test 2 | Test 3 | Test 4 | Test 5 | Average |
|---|---|---|---|---|---|---|
| **Density ($\rho_G$)** | 1.70 | 1.70 | 1.70 | 1.71 | 1.69 | 1.70±0.01 |
| **Open porosity** | 23.84% | 23.39% | 24.51% | 23.92% | 23.53% | 23.8±0.43% |
| **Total porosity** | 25.17% | 25.14% | 24.82% | 24.45% | 25.46% | 25.0±0.4% |
| $\rho_S$ | 2.23 | 2.21 | 2.26 | 2.25 | 2.21 | 2.23±0.02 |
| **$V_p$ max (*mL/g*)** | 0.141 | 0.138 | 0.144 | 0.140 | 0.139 | 0.140±0.002 |

TABLE 16: RAW RESULTS OF MERCURY MEASUREMENTS ON VIRGIN GRAPHITE SAMPLES OF THE G2 REACTOR ($V_P$ POROUS VOLUME PER GRAM OF GRAPHITE)

The results shown in the previous table were obtained by taking into account the entire sequence of analyses up to a total pressure of 400 MPa. The values are deduced from the volume of mercury that penetrated the sample up to that pressure. It is worth noting that, under such conditions, the measured skeleton density is very close to the theoretical density of graphite, which leads to an open porosity close to total porosity and to a closed porosity equal to 0. Those contradictory results with the previous helium-pycnometry output show that the pressures (400 MPa) achieved by helium intrusion have modified the porous network by opening the sealed porosity.

For the rest of this study, we have decided to interpret the helium-porosimetry results up to an injection pressure of 12 MPa (i.e., half of the mechanical strength of graphite) for graphite, thus corresponding to pores with a bore-mouth radius of about 0.1 µm. The recalculated skeleton densities for that pressure limit are then consistent with helium measurements (Table 17).

| Sample | Test 1 | Test 2 | Test 3 | Test 4 | Test 5 | Average |
|---|---|---|---|---|---|---|
| Size/pressure | 0.1 µm 12 MPa | 0.1 µm 12 MPa | 0.1 µm 12 MPa | 0.1 µm 12 MPa | 0.1 µm 12 MPa | 0.1 µm 12 MPa |
| **Density ($\rho_G$)** | 1.70 | 1.70 | 1.70 | 1.71 | 1.69 | 1.70±0.01 |
| **Open porosity** | **19.8%** | **19.5%** | **21.5%** | **20.5%** | **19.6%** | 20.2±0.9% |
| **Total porosity** | 25.17% | 25.14% | 24.82% | 24.45% | 25.46% | 25.0±0.4% |
| **$\rho_S$** | **2.11** | **2.10** | **2.15** | **2.13** | **2.10** | 2.12±0.02 |
| **$V_p$ max (*mL/g*)** | 0.1167 | 0.1129 | 0.1225 | 0.1139 | 0.116 | 0.116 |

TABLE 17: RESULTS OF MERCURY MEASUREMENTS FOR AN INJECTION PRESSURE BELOW 12 MPA

Data relating to pore-size distribution in relation to porosity accessible to helium distribution are presented in Table 18 by adopting a cutting zone at 0.1 µm.

| Pore size | >30 µm | 1 to 30 µm | 0.1 to 1 µm |
|---|---|---|---|
| **Pressure (*MPa*)** | 0-0.035 | 0.035-1.24 | 1.24-12.4 |
| **Test P** | 4% | 75% | 19% |
| **Test 2** | 1% | 78% | 20% |
| **Test 3** | 0.4% | 78% | 18% |
| **Test 4** | 6% | 68% | 20% |
| **Test 5** | 4% | 76% | 19% |
| **Average** | **3.0±2.2%** | **75±4%** | **19±0.4%** |

TABLE 18: DISTRIBUTION OF APPARENT DIAMETERS FOR G2 VIRGIN GRAPHITE PORES

Pores located in the zone ranging from 1 to 30 µm amount to approximately 75% of the total with the maximum distribution oscillating towards 3.5 µm.

## 6.4. Summary

In conclusion, lamellae Nos. 1 and 4, as well as the block of the inactive G2 graphite brick have the characteristics shown in Table 19.:

| | **Lamella No. 1 (*LPCMI*)** | **Lamella No. 4 (*LARC/LECD*)** | **Block** |
|---|---|---|---|
| **Density (*edge*)** | 1.65 | 1.72±0.05 (n=8) | |
| **Total porosity (*edge*)** | 27.2±0.7% | 23.9±0.7% (n=8) | |
| **Open porosity (*edge*)** | 24.7% (n=2 for He) | Not measured | |
| **Sealed porosity (*edge*)** | 3.22%(n=2 for He) | Not measured | |
| **Core density** | 1.59 | 1.66±0.07 (n=11) | |
| **Total porosity (*core*)** | 29.8±0.9% (n=20)<br>33.32% (n=2 for He) | 26.9±0.9% (n=11)<br>25.6±0.9% (n=1 for He) | |
| **Open porosity (*core*)** | $Po_{(He)}$ = 30.4%<br>(n=2 pour He) | $Po_{(He)}$ = 21.7±1.2%<br>(n=1 for He) | |
| **Sealed porosity (*core*)** | 2.9%<br>(n=2 for He) | 3.9 ± 1.5%<br>(n=1 for He) | |
| | | | |
| **Average density** | 1.63 (n=34) | 1.68±0.08 (n=25) | 1.717±0.009 |
| **Total porosity** | 28.3% (n=34) | 25.8% (n=25) | 24.2±0.05% |
| **Porosity** | | Macroporous solid | |
| **Pore-size distribution** | | # 4% > at 30 µm<br># 75% between 1 and 30 µm<br># 19% between 0.1 and 1µm | |

TABLE 19: CHARACTERISTICS OF G2 VIRGIN BRICK

Summary results clearly show that graphite is an essentially heterogeneous solid from a microstructural point of view (density, porosity) at the scale of centimetric samples. Results highlight impregnation differences between the edge and the core of the brick, thus reflecting a higher open porosity in the brick core, while the sealed porosity remains constant between 3 and 4 %. Pore size lies essentially between 1 and 30 µm, with the maximum distribution at 3.5 µm. The helium-porosimetry technique is not able to determine pore distribution below 0.1 µm.

## 6.5. X-ray diffraction

Three samples collected on the surface of lamella No. 1 of the non-irradiated G2 brick were characterised at the LPCMI by X-ray diffraction in order to determine the *a* and *c* meshing parameters, as well as the full width at half-maximum (FWHM) of diffraction peaks. The purpose of those determinations is to provide reference values to be compared with the values resulting from irradiated samples and, thus, to determine the crystalline evolution of G2 graphite under irradiation (potential mesh swelling/deformation and evolution of the size of graphite crystallites).

Since the anisotropic nature of graphite is also reinforced by the extrusion process due to its crystalline structure, the three G2 samples that were characterised by X-ray diffraction were collected in the three major directions of the brick in order to detect potential differences (Figure 5): X1-1, perpendicular to extrusion; Y3-2: perpendicular to extrusion, and Z1-1, parallel to extrusion.

X-ray-diffraction recordings are representative of Fact Sheet No. 74-2330 of the International Centre for Diffraction Data (ICDD) relating to graphite (Annex 1). The expansion of the zone containing the main peak – (002) – displays a significant dissymmetry in the diffraction peaks of all characterised samples. Since graphite is a slightly dense material, X rays penetrate deep inside the samples, thus inducing an asymmetrical expansion of diffraction peaks (absorption effect). The resulting diffractograms also clearly show a marked crystallographic texture to be tied directly with the forming process by extrusion (Figure 16). Hence, it appears that peaks (002), (004) and (006) are more intense for samples X1-1 and Y3-2 than for sample Z1-1, which reflects the fact that the basic planes of graphite crystal – peaks (002), (004) and (006) – and by par analogy, the coke grains, are preferentially oriented according to the extrusion axis of the brick.

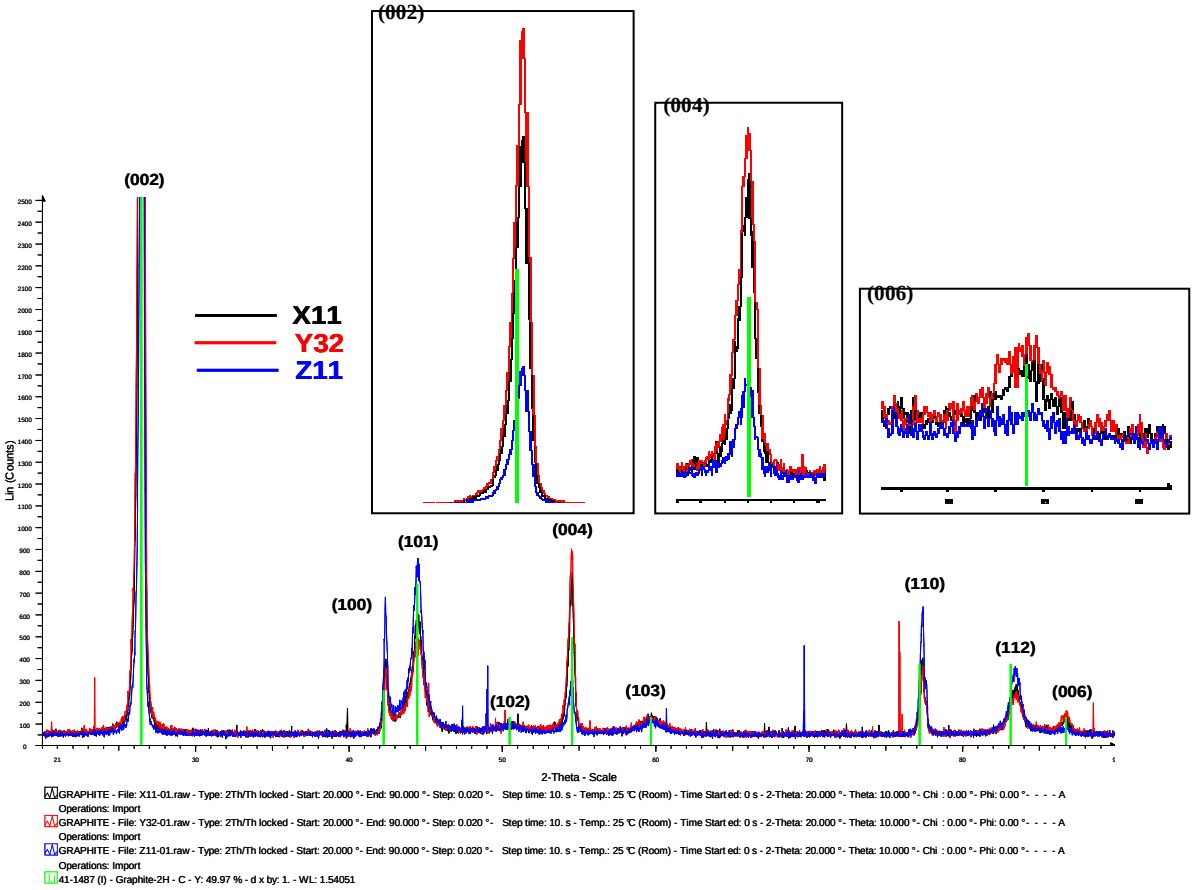


FIGURE 16: DIFFRACTOGRAMS OF G2 VIRGIN GRAPHITE SAMPLES

Analysing the recorded diffractograms leads to meshing parameters and diffraction-peak FWHMs (002), (004) and (110), as presented in Tables 20 and 21.

| G2 | Parameter *c* (*Å*) | Parameter *a* (*Å*) |
|---|---|---|
| **Theoretical parameters** | 6.707 | 2.461 |
| **X1-1 (⊥)** | 6.725 ± 0.002 | 2.460 ± 0.002 |
| **Y3-2 (⊥)** | 6.725 ± 0.002 | 2.460 ± 0.002 |
| **Z1-1 (//)** | 6.738 ± 0.002 | 2.461 ± 0.002 |

TABLE 20: MESHING PARAMETERS OF G2 VIRGIN GRAPHITE

| G2 | (hkl) | Peak position (°) | FWHM (°) |
|---|---|---|---|
| X1-1 | (002) | 26.49 | 0.30 |
| | (004) | 54.54 | 0.43 |
| | (110) | 77.55 | 0.58 |
| Y3-2 | (002) | 26.49 | 0.31 |
| | (004) | 54.54 | 0.45 |
| | (110) | 77.55 | 0.61 |
| Z1-1 | (002) | 26.43 | 0.24 |
| | (004) | 54.42 | 0.53 |
| | (110) | 77.44 | 0.84 |

TABLE 21: FWHM OF PEAKS (002), (004) AND (110) OF G2 VIRGIN GRAPHITE

In the light of *a* parameter values (quasi identical to those of graphite monocrystal), the samples from lamella No. 1 of the G2 brick seem to include a very good organisation of graphene planes. It should be noted that the layout of the carbon atoms in the hexagonal structure ($sp^2$ carbon) requires no considerable energy input, hence, even for relatively low graphitisation temperatures, any carbonated material will still have graphene-type planes. However, with regard to *c* parameter values, they are further away from that of graphite monocrystal, which tends to prove that graphitisation was not thorough – a common phenomenon for industrial graphite. In fact, establishing the three-dimensional structure of graphite requires higher temperatures than 3,000°C, whereas a temperature of 2,700-2,800°C is sufficient for most fabrication processes.

If we compare the meshing parameters between the different samples, the value of the *c* parameter associated with sample Z1-1 varies slightly from that of the samples collected perpendicularly to the direction of the extrusion. That may be explained by the fact that, when the graphite is formed, radial-compression stresses are introduced in the graphite with a decreasing gradient at the surface towards the block core. Since the chemical bond between the graphene planes is relatively poor (Van-der-Waals-type bonding), the presence of radial compression stresses modifies slightly the value of the *c* parameter. For samples X1-1 and Y3-2, the graphene planes analysed by X-ray diffraction are mainly oriented in such a way for radial compression stresses to close up (decrease of *c*). For sample Z1-1, graphene planes are primarily oriented in such a way for radial compression stresses to distance themselves from each other (increase of *c*).

Since the chemical bonds within graphene planes are very strong, the compression stresses created during graphite extrusion are not important enough to induce a significant change of the crystalline *a* parameter.

The values of diffraction-peak FWHM values presented in Table 21 do not raise any specific comment and serve merely as reference data to be compared to the values achieved on irradiated samples.

## 6.6. Raman spectroscopy

The three samples that were studied by X-ray diffraction were also characterised at the LPCMI by Raman microspectroscopy. That analytical technique, just as X-ray diffraction, is designed for the crystalline study of matter, but at a more local scale. While X-ray diffraction integrates the information over approximately 1 $cm^2$, Raman microspectrometry focuses on an area covering 2 to 3 $\mu m^2$. Beyond providing information on the crystalline structure of the materials, Raman spectroscopy also displays the crystalline faults of the sample. In fact "pure" graphite has a single Raman band (marked Band G) located at about 1580 $cm^{-1}$. If crystalline faults are present in the structure, three additional bands are likely to appear: Band D1 (~1360 $cm^{-1}$), Band D2 (~1,620 $cm^{-1}$) and Band D3 (~1,540 $cm^{-1}$).

Since that technique is very local and graphite is more a composite than a homogeneous material (coke grains, binding agent, impregnation pitch), two zones were characterised for each of the three samples :

- the cleaved part of a coke grain, the most "graphited zone of the sample (Figure 17a), and
- the external face of a coke grain, a zone where are located notably the binding agent and the impregnation pitch, two materials that are twice as less "graphitable" as coke and, hence, have a graphitic structure of lesser quality (Figure 17b).

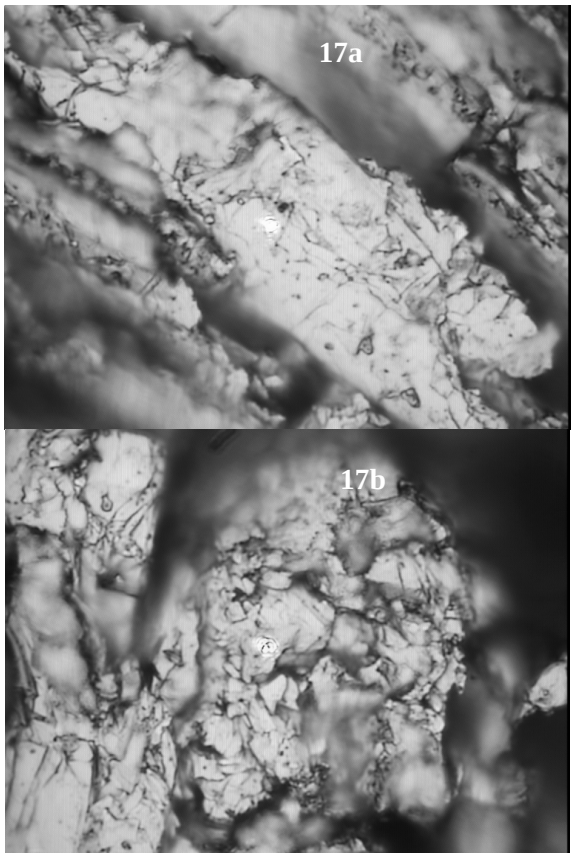


FIGURE 17: RAMAN MICROSCOPE WITH AN X100 LENS

As expected, the acquisitions made on the cleaved section and the external face of coke grains lead to different Raman spectra (Figure 18). Hence, the cleaved part of the grain also has a quasi-perfect graphitic structure: Band G of the graphite at 1580 $cm^{-1}$ with a very slightly intense Band D1 (with the Bands D2 and D3 not being visible). However, the spectrum achieved outside of the coke grain spectrum clearly shows the presence of Bands D1 and D2, whereas Band D3 is more difficult to display. All recorded Raman spectra are shown in Annex 2.

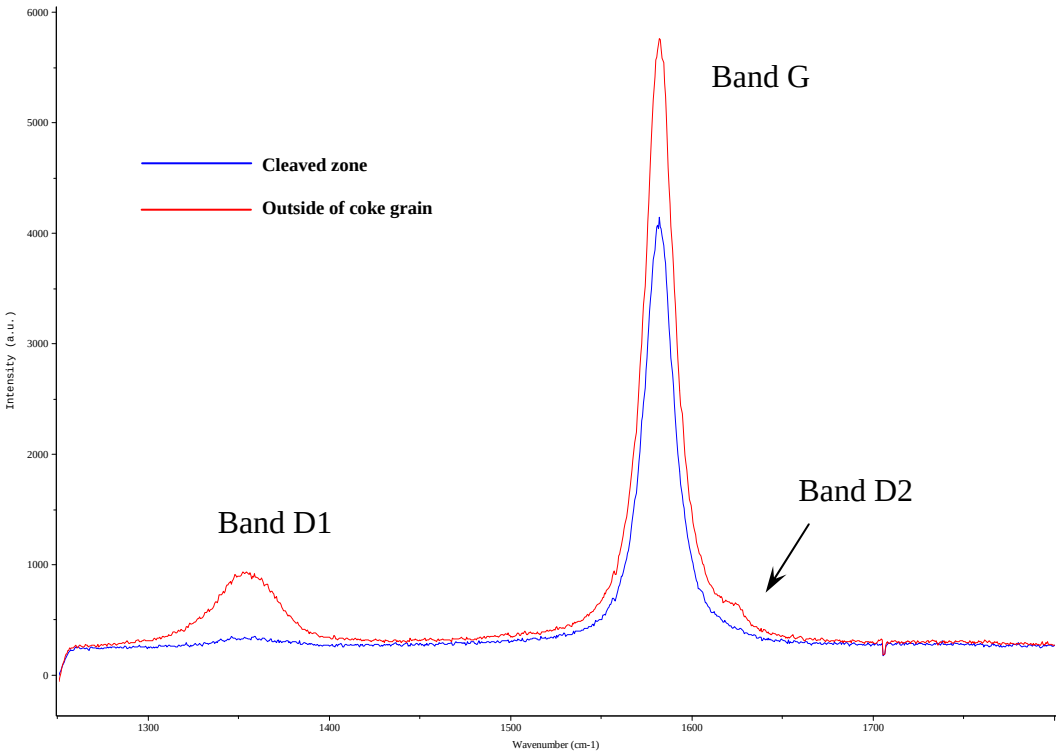


FIGURE 18: RAMAN RANGES OF SAMPLE X1-1

If the acquisitions made on the cleaved part of the coke grains of samples X1-1, Y3-2 et Z1-1 lead to identical Raman spectra (Figure 19), the spectra resulting from the acquisitions made outside the grains a re less similar (Figure 20). That phenomenon may be explained by the fact that, since coke grains are “well graphitable”, their internal structure is almost identical from one grain to another, thus generating superimposed Raman spectra. However, the zones being analysed outside the grains may vary locally (+/- binding agent or impregnation pitch at various graphitation levels), which might lead to relative intensities between flaw bands and Band G, which vary among spectra.

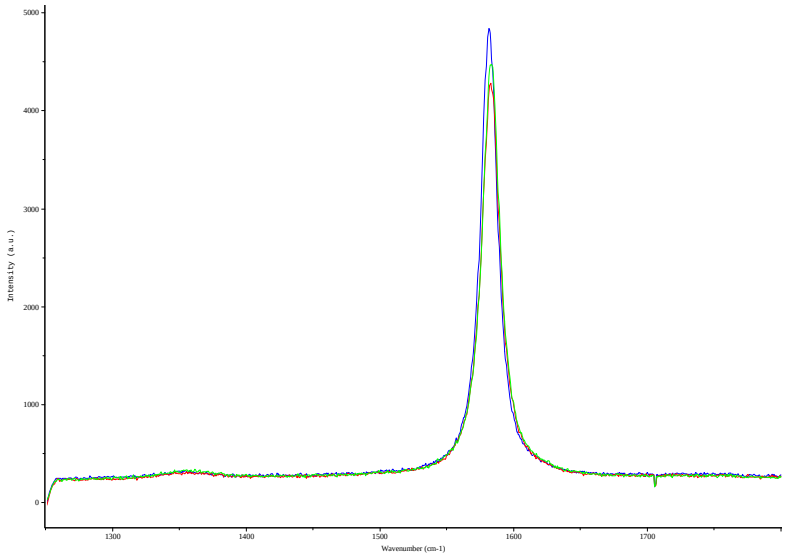


FIGURE 19: RAMAN RANGES FOR SAMPLES X1-1, Y3-2 AND Z1-1 (CLEAVED ZONE)

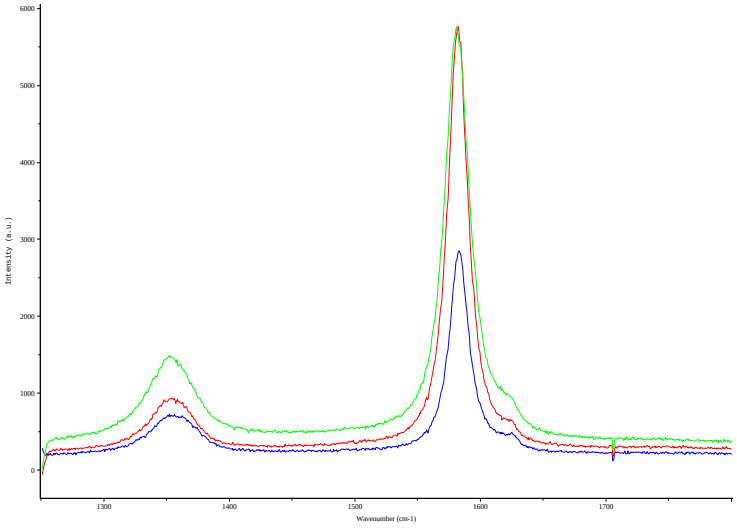


FIGURE 20: RAMAN RANGES FOR SAMPLES X1-1, Y3-2 AND Z1-1 (EXTERNAL GRAINS)

The deconvolution of the Raman spectra made for different samples led to the results presented in Table 22. Those data, and notably the intensity ratios of the flaw bands and Band G, will serve as reference to be compared with the data obtained on irradiated G2 samples. It was noted naturally that the value of the intensity ratio of Bands D and G is proportionally lower, if the analysed zone is well crystallised.

Those deconvolutions were also useful in confirming the visual observations of the Raman spectra outside the coke grains, or in other words, that it was not possible to detect the contribution of D3 flaw bands in the recorded spectra (Figure 21). Deconvolutions relating to the other Raman spectra are shown in Annex 3.

| | | Band G | | | Band D1 | | | Band D2 | | | A(D1)/A(G) | A(D2)/A(G) |
|---|---|---|---|---|---|---|---|---|---|---|---|---|
| | | Position | Intensity | Area | Position | Intensity | Area | Position | Intensity | Area | | |
| X-11 | Coke | 1,583 | 4,051 | 18,5377 | 1,358 | 49 | 4,289 | | | | 0.0023 | |
| | Ext grain | 1,582 | 5,487 | 29,3158 | 1,354 | 653 | 59,910 | 1,623 | 119 | 3,066 | 0.204 | 0.215 |
| Y-32 | Coke | 1,583 | 4,255 | 19,1380 | 1,358 | 71 | 75,553 | | | | 0.038 | |
| | Ext grain | 1,581 | 5,358 | 34,6094 | 1,353 | 1037 | 108,202 | 1,621 | 225 | 8,923 | 0.313 | 0.338 |
| Z-11 | Coke | 1,581 | 4,605 | 19,1997 | 1,354 | 45 | 402 | | | | 0.018 | |
| | Ext grain | 1,582 | 2,628 | 13,8313 | 1,355 | 495 | 47,956 | 1,623 | 120 | 4,469 | 0.347 | 0.379 |
| *Average* | Coke | 1582 | 4304 | 189,585 | 1,357 | 55 | 5,015 | | | | 0.026 | |
| | Ext grain | 1582 | 4491 | 259,188 | 1,354 | 726 | 72,023 | 1,622 | 155 | 5,486 | 0.278 | 0.299 |

TABLE 22: RAMAN DATA RELATING TO G2 NON-IRRADIATED SAMPLES

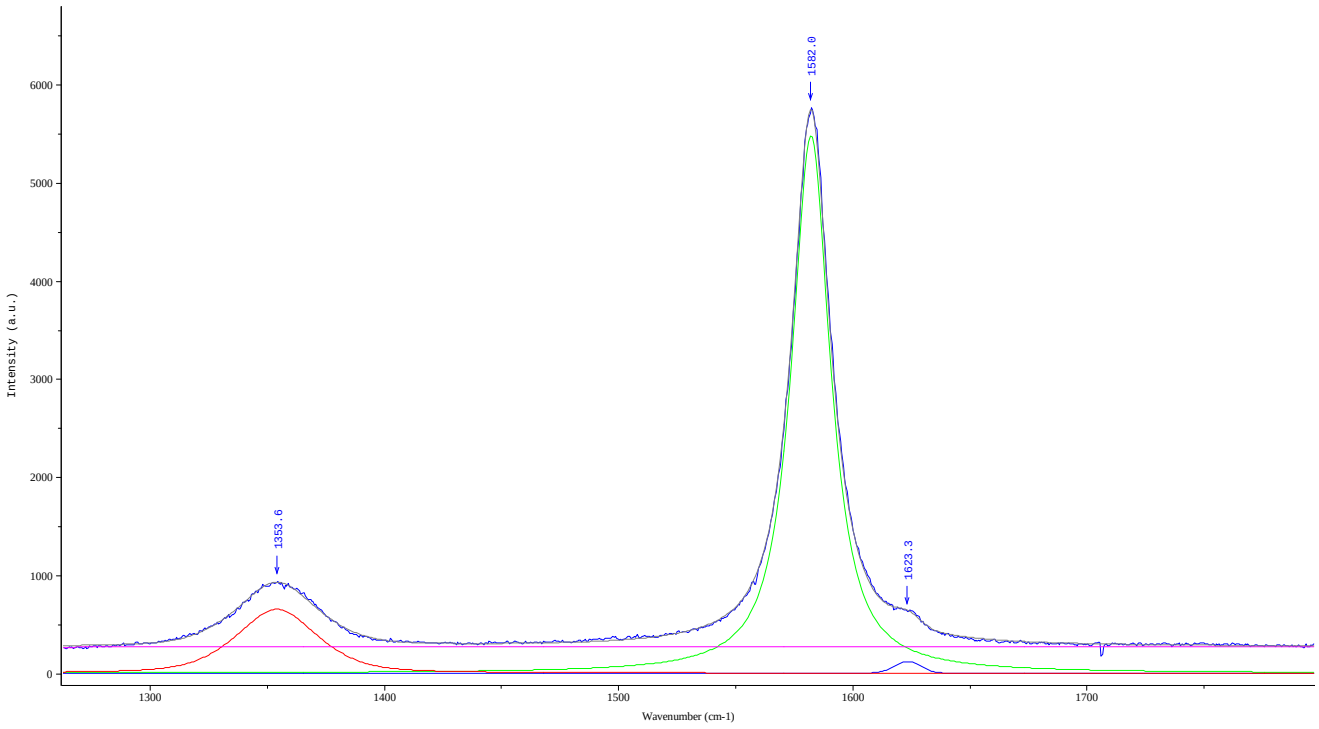


FIGURE 21: DECONVOLUTION OF THE RAMAN RANGE IN SAMPLE ***échantillons*** X1-1 (EXTERNAL GRAINS)

# 7 Results on irradiated G2 samples

As mentioned in Section 4 (“Preparation of samples”), G2 graphite cores were recut and distributed between both laboratories (see Table 7), as follows:

- cutting waste was used for porosity-characterisation purposes at Cadarache. Hence, for every core, porosity measurements by helium pycnometry were made on three locations on the core: at both extremities and in the middle. In the case of geometric-density measurements, the samples that were prepared for leaching tests were used, because cutting waste is unable to provide a reliable geometric-density value (complex form and small sample). Those samples were all collected towards the middle (i.e., between both channels),
- at Saclay, the geometric-density measurements were taken on samples with a compatible geometry, which include samples G2-27-3, G2-27-4, G2-27-5, G2-32-3, G2-32-4, G2-42-3, G2-42-4, G2-46-2 and G2-46-3 (Figures 8 and 9). Hydrostatic densities were determined with bromobenzene on samples measuring 10 mm in diameter by 10 mm in height that were cored from samples G2-27-3, G2-32-3, G2-42-3 and G2-46-2 respectively.

## *7.1. Geometric-density measurements*

The geometric density readings from prismatic (Table 23) and cylindrical (Table 24) lamellae are consistent for all samples.

| Item n° | Mass | Average size (*cm*) | | | $\rho_G$ | Total porosity | Remarks |
|---|---|---|---|---|---|---|---|
| | (g) | L | l | H | | % | |
| **G2-27-7A** | 12.1629 | 1.53 | 1.53 | 3.02 | 1.72±0.03 | 24.1±0.3 | Leaching balance |
| **G2-27-7B** | 10.0860 | 1.62 | 1.51 | 2.46 | 1.67±0.04 | 26.2±0.3 | |
| **G2-27-7C** | 12.0563 | 1.61 | 1.51 | 3.01 | 1.65±0.04 | 27.0±0.3 | |
| **G2-27-7D** | 6.1674 | 1.52 | 1.52 | 1.67 | 1.60±0.04 | 29.2±0.3 | Initial SIMS |
| **G2-27-7E** | 1.0933 | 0.91 | 0.47 | 1.52 | 1.68±0.08 | 25.8±0.6 | ½ cut for SIMS measurement |
| ***Average*** | | | | | *1.67±0.05* | | |
| ***Minimum*** | | | | | *1.60±0.04* | | |
| ***Maximum*** | | | | | *1.72±0.03* | | |
| **G2-32-6A** | 10.5228 | 1.47 | 1.46 | 3.12 | 1.58±0.04 | 30.0±0.4 | Leaching balance |
| **G2-32-6B** | 8.2873 | 1.46 | 1.41 | 2.51 | 1.61±0.04 | 28.7±0.4 | |
| **G2-32-6C** | 10.6187 | 1.48 | 1.42 | 3.15 | 1.61±0.04 | 29.1±0.4 | |
| **G2-32-6D** | 10.3788 | 1.48 | 1.41 | 3.12 | 1.60±0.04 | 29.4±0.4 | Initial SIMS |
| **G2-32-6E** | 1.0243 | 0.82 | 0.53 | 1.41 | 1.67±0.08 | 26.2±0.6 | ½ cut for SIMS measurement |
| ***Average*** | | | | | *1.61±0.04* | | |
| ***Minimum*** | | | | | *1.58±0.04* | | |
| ***Maximum*** | | | | | *1.67±0.08* | | |
| **G2-42-6A** | 13.2756 | 1.61 | 1.52 | 3.12 | 1.74±0.06 | 23.3±0.4 | Leaching balance |
| **G2-42-6B** | 9.8308 | 1.48 | 1.53 | 2.57 | 1.70±0.04 | 25.1±0.3 | |
| **G2-42-6C** | 13.1417 | 1.53 | 1.64 | 3.12 | 1.68±0.04 | 25.8±0.3 | |
| **G2-42-6D** | 3.6458 | 1.43 | 1.01 | 1.53 | 1.66±0.05 | 26.9±0.4 | Initial SIMS |
| **G2-42-6E** | 1.1327 | 0.78 | 0.55 | 1.53 | 1.73±0.08 | 23.8±0.6 | ½ cut for SIMS measurement |
| ***Average*** | | | | | *1.70±0.05* | | |
| ***Minimum*** | | | | | *1.66±0.05* | | |
| ***Maximum*** | | | | | *1.74±0.06* | | |
| **G2-46-5A** | 11.9283 | 1.6 | 1.48 | 3.02 | 1.67±0.03 | 26.4±0.4 | Leaching balance |
| **G2-46-5B** | 9.6695 | 1.62 | 1.47 | 2.49 | 1.64±0.04 | 27.7±0.3 | |
| **G2-46-5C** | 11.9511 | 1.62 | 1.49 | 3.06 | 1.62±0.04 | 28.6±0.3 | |
| **G2-46-5D** | 11.5513 | 1.58 | 1.46 | 3.05 | 1.65±0.04 | 27.3±0.3 | Initial SIMS |
| **G2-46-5E** | 1.0066 | 0.79 | 0.48 | 1.59 | 1.67±0.08 | 26.3±0.3 | ½ cut for SIMS measurement |
| ***Average*** | | | | | *1.65±0.04* | | |
| ***Minimum*** | | | | | *1.62±0.04* | | |
| ***Maximum*** | | | | | *1.67±0.08* | | |

TABLE 23: GEOMETRIC-DENSITY MEASUREMENT ON G2 PRISMATIC IRRADIATED SAMPLES

| Core | Sample (see cutting plan) | Median diameter (cm) (±0.02) | Median thickness (cm) (±0.02) | Mass (g) | Density (±0.02) | Total porosity (%) (±0.4%) | Wear (% (±0.8%) |
|---|---|---|---|---|---|---|---|
| G2-27 | 3 | 6.32 | 1.10 | 56.3001 | 1.62±0.02 | 28.51 | 5.26 |
| | 4 | 6.33 | 0.96 | 49.6919 | 1.65±0.02 | 27.18 | 3.51 |
| | 5 | 6.32 | 3.02 | 157.2170 | 1.66±0.02 | 26.74 | 2.92 |
| | 6 | 6.32 | 1.53 | 80.0304 | 1.67±0.02 | 26.4 | 2.5 |
| G2-32 | 3 | 6.33 | 1.08 | 54.8243 | 1.62±0.02 | 28.51 | 5.26 |
| | 4 | 6.32 | 2.91 | 147.8640 | 1.62±0.02 | 28.51 | 5.26 |
| | 5 | 6.32 | 1.40 | 72.0947 | 1.64±0.02 | 27.6 | 4 |
| G2-42 | 3 | 6.32 | 1.09 | 58.6864 | 1.71±0.02 | 24.54 | 0.00 |
| | 4 | 6.32 | 3.04 | 164.6040 | 1.73±0.02 | 23.65 | -1.17 |
| | 5 | 6.32 | 1.50 | 82.044 | 1.74±0.02 | 23.1 | -2 |
| G2-46 | 2 | 6.33 | 1.05 | 55.4287 | 1.69±0.02 | 25.42 | -0.60 |
| | 3 | 6.34 | 3.03 | 159.2290 | 1.67±0.02 | 26.30 | 0.60 |
| | 4 | 6.32 | 1.56 | 80.8629 | 1.65±0.02 | 27.1 | 1.6 |

TABLE 24: GEOMETRIC DENSITY MEASUREMENTS ON IRRADIATED CYCLINDRICAL G2 SAMPLES

*For calculating the wear rate of "Special" coke A reference: 1.71- ref Lockport coke: 1.68*

Results show that irradiated graphite samples have slightly lower densities than those of virgin graphite, except for G2-42 and G2-46 cores, whose density may be considered as identical to that before irradiation (« Special » Grade-A coke moderator: 1.71 and Lockport coke reflector: 1.68). That reduction in density is due to graphite wear under irradiation (radiolytic corrosion).

The wear is consistent with the neutron-creep level received by the samples and measured activities.

| | Order |
|---|---|
| **Neutron creep** | G2-32~G2-27 > G2-42 > G-46 |
| **Measured wear (%)** | G2-32 > G2-27 > G2-42 > G-46 |

TABLE 25: CLASSIFICATION OF SAMPLES IN RELATION TO NEUTRON CREEP, WEAR AND MEASURED ACTIVITY (IN DECREASING ORDER)

However, caution is called for concerning the link between the collection zone and the activity of the samples. In fact, their activity depends on neutron creep (possible correlation with the position of the samples in the core), but it also depends on the impurities contained in the samples and likely to be activated, since the distribution of those impurities may be quite heterogeneous among bricks or even within the same brick.

Caution is also advised for the fine quantification of graphite-density variations in relation to the location of the samples and with due account of the small evolutions being recorded in comparison with the disparities in the values being observed not only on virgin materials (difference between edge and core densities) and irradiated materials. However, it is possible to propose the existence of a radial geometric-density gradient between the core and the channel of the bricks for the three moderator samples (Figure 22). That gradient seems all the more significant (G2-27) since the sample has received a high neutron creep, which is consistent with the more intense radiolytic corrosion at the edge of the bricks.

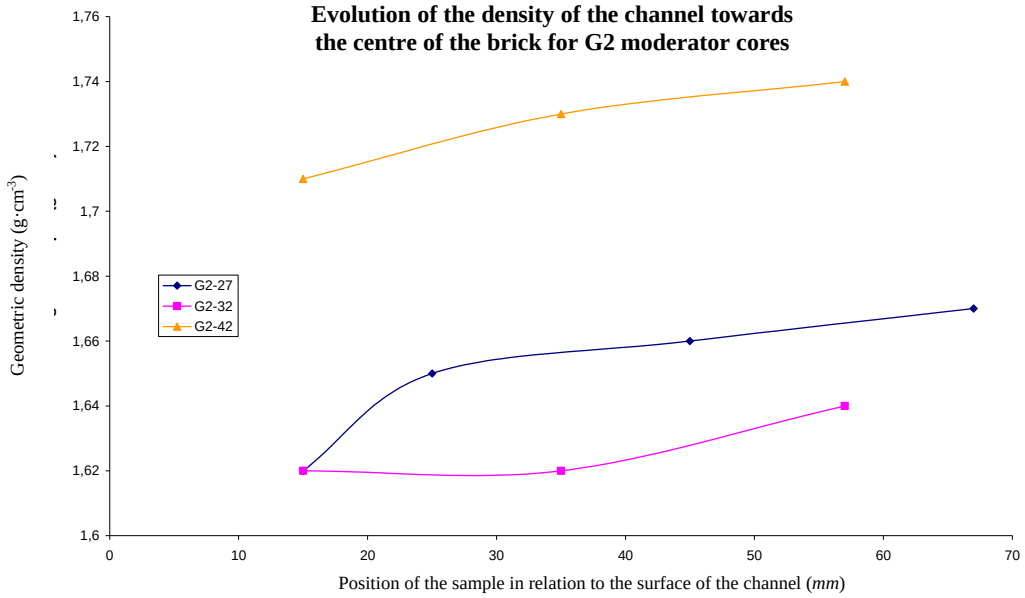


FIGURE 22: EVOLUTION OF DENSITY WITHIN THE SAME G2 CORE

## 7.2. Open-porosity measurements: hydrostatic density by bromobenzene and helium pycnometry

The hydrostatic density measurements at LPCMI were made in bromobenzene after vacuum imbibition of the samples. The resulting values correspond to the density of the carbonated graphite skeleton and allow for reaching the percentage of open and sealed porosities of G2 irradiated samples. The results of hydrostatic densities are shown in Table 26.

At the LARC, the G2 samples being analysed by helium pycnometry have a mass of approximately 10 g and have been collected from the extremities and the middle of each sample. The measuring error is estimated at 4%. On the basis of the geometric densities and the density measurements of skeletons, it is possible to deduce the total, open, as well as sealed porosities of the samples thanks to formulae (8), (9) and (10), respectively.

| **Hydrostatic density ($\rho_S$)** | | | |
|---|---|---|---|
| **Sample** | ***Measurement 1*** | ***Measurement 2*** | ***Average*** |
| **G2-27-3-1** | 2.180 | 2.181 | 2.18 ± 0.05 |
| **G2-32-3-1** | 2.190 | 2.191 | 2.19 ± 0.05 |
| **G2-42-3-4** | 2.181 | 2.182 | 2.18 ± 0.05 |
| **G2-46-2-1** | 2.126 | 2.128 | 2.13 ± 0.05 |

TABLE 26: HYDROSTATIC DENSITY AT LPCMI ON IRRADIATED G2 SAMPLES

| Sample | Average density ($\rho_G$) | $\rho_S$ Helium or bromobenzene | Total porosity Ref *d=2.266* | Open P (Ref.) Average/ measured density | Sealed porosity |
|---|---|---|---|---|---|
| **Virgin** (core lamella No. 4) | 1.69±0.06 | 2.15±0.05(1) | 25.6±0.9% | 21.7±1.2% | 4.9±1.4% |
| **Virgin** (core lamella No. 1) | 1.57±0.05 | 2.17±0.05(1) | 30.7±1.0% | 27.6±1.1% | 3.1±1.5% |
| **G2-27-1** | 1.67±0.05 | 2.17±0.09(1) | 26.3±0.6% | 22.9±1.1% | 3.4±1.2 |
| **G2-27-3-1** | 1.62±0.02 | 2.18±0.05(2) | 28.5±0.4% | 25.7±0.7% | 2.8±0.8 |
| **G2-27-7** | 1.65±0.05 | 2.27±0.09(1) | 27.2±0.7% | 27.3±1.3% | -0.1±1.4% |
| **G2-27-8** | 1.68±0.05 | 2.22±0.09(1) | 25.9±0.6% | 24.3±1.1% | 1.7±1.3% |
| **G2-32-1** | 1.67±0.05 | 2.16±0.09(1) | 26.5±0.7% | 22.9±1.1% | 3.5±1.3% |
| **G2-32-3-1**(2) | 1.62±0.02 | 2.19±0.05(2) | 28.5±0.4% | 26.0±0.7% | 2.5±0.8% |
| **G2-32-6** | 1.65±0.05 | 2.18±0.09(1) | 27.1±0.7% | 24.3±1.1% | 2.8±1.3% |
| **G2-32-7** | 1.67±0.05 | 2.17±0.09(1) | 26.4±0.7% | 23.0±1.1% | 3.4±1.3% |
| **G2-42-1** | 1.71±0.05 | 2.11±0.09(1) | 24.5±0.7% | 19.1±0.9% | 5.4±1.2% |
| **G2-42-3-4** (2) | 1.71±0.02 | 2.18±0.05(2) | 24.5±0.3% | 21.6±0.6% | 3.0±0.6% |
| **G2-42-6** | 1.69±0.05 | 2.17±0.09(1) | 24.3±0.7% | 20.8±1.0% | 4.9±1.1% |
| **G2-42-7** | 1.70±0.05 | 2.14±0.09(1) | 24.8±0.7% | 20.5±1.0% | 5.8±1.1% |

TABLE 27: RESULTS OF HELIUM/BROMOBENZENE-PYCNOMETRY MEASUREMENTS FOR THE GRAPHITE OF THE IRRADIATED G2 MODERATOR

*(1) Skeleton density determined by helium pycnometry.*
*(2) Skeleton density determined by bromobenzene imbibition.*

Table 28 shows the results for the reflector sample (G2-46).

| Sample | Average density $\rho_G$ | $\rho_S$ He or bromobenzene | Total porosity Ref d=2.266 | Open P (Ref.) Average/ measured density | Sealed porosity |
|---|---|---|---|---|---|
| **Raw** [8] **(Lockport – attention ref. (*Hg*))** | **1.68±0.06** | **–** | **25.38%** | **21.42%** | **3.96%** |
| **G2-46-1** | 1.68±0.05 | 2.14±0.09(1) | 25.9±0.6% | 21.5±1.0% | 4.4±1.2% |
| **G2-46-2-1** (2) | 1.69 ±0.02 | 2.13±0.05(2) | 25.4±0.3% | 20.7±0.5% | 4.8±0.6% |
| **G2-46-5** | 1.69±0.05 | 2.13±0.09(1) | 25.6±0.6% | 20.7±1.0% | 4.9±1.1% |
| **G2-46-6** | 1.69±0.05 | 2.10±0.09(1) | 25.5±0.6% | 19.7±0.9% | 5.8±1.1% |

TABLE 28: RESULTS OF HELIUM-PYCNOMETRY MEASUREMENTS OF GRAPHITE FOR THE IRRADIATED G2 REFLECTOR

*Reference data on virgin graphite resulting from Reference*[8] *: (1) Skeleton density as determined by helium pycnometry.*
*(2) Skeleton density as determined by bromobenzene.*

It was observed that, in the case of the G2-moderator samples collected in the nearest zones to the reactor core (G2-27 and G2-32), not only the total porosity, but also the open porosity, had increased, whereas the sealed porosity has decreased. That observation is consistent with the literature[16] [17] and may be explained by the fact that radiolytic corrosion within a $CO_2$ atmosphere induces the opening of the porosity that was not reached initially by helium and/or bromobenzene, hence an increase of the open porosity and a reduction of the sealed porosity.

Since sample No. 42 was the first moderator core at the limit of the reflector, and thus the most distant from the core, it was less irradiated and was exposed to a lower temperature than the two others. Consequently, the porosity values are almost identical to those that were determined on the inactive brick, which confirms the previous observations on the evolution of the geometric density and leads to the conclusion that radiolytic corrosion may be considered as negligible with regard to the zone of the G2 moderator.

Open-porosity calculations show also that the open porosity of the extremities of cores G2-27 and G2-32 is lower than that of the sample taken from the brick core and of virgin samples. However, the gradient is lower for irradiated samples (2%) than for virgin samples (5%), thus confirming that radiolytic corrosion acts primarily on the edge of the brick.

For the reflector sample, measurements show that open and sealed porosities have the same order of magnitude, irrespective of the position of the core and are close to the data gathered from the literature for a non-irradiated sample. Hence, it may be concluded that irradiation damages in that zone are very small.

## 7.3. Mercury porosimetry

Figure 23 shows the evolution of the porous volume in relation to pore-diameter and pore-distribution results at the LARC for the samples of irradiated graphite and for the three positions of each core, respectively. The tests were conducted with helium porosimetry in a glove box at the CHICADE Facility.

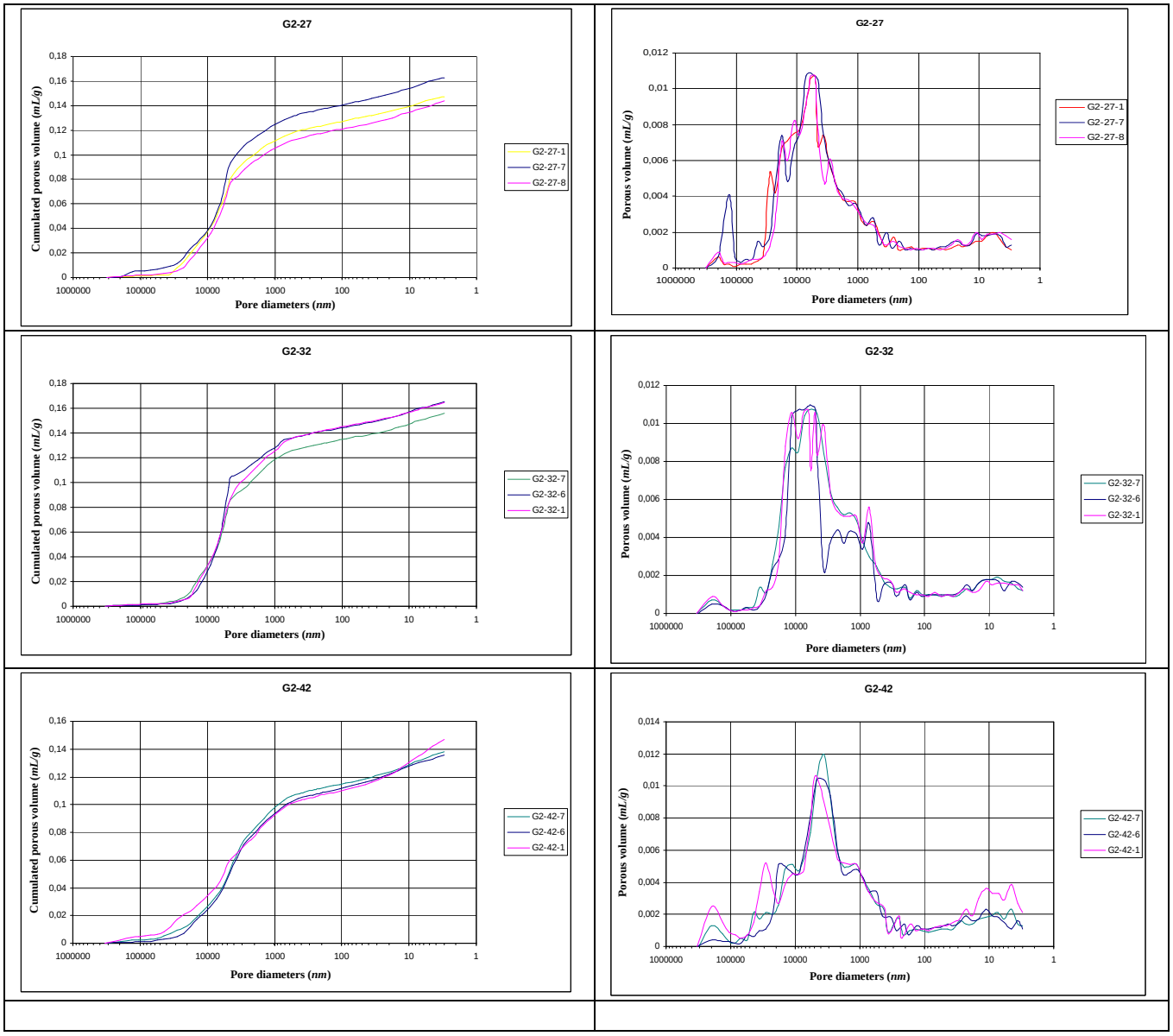


FIGURE 23: MERCURY-POROSITY RANGE OF ACTIVE G2 REFLECTOR SAMPLES

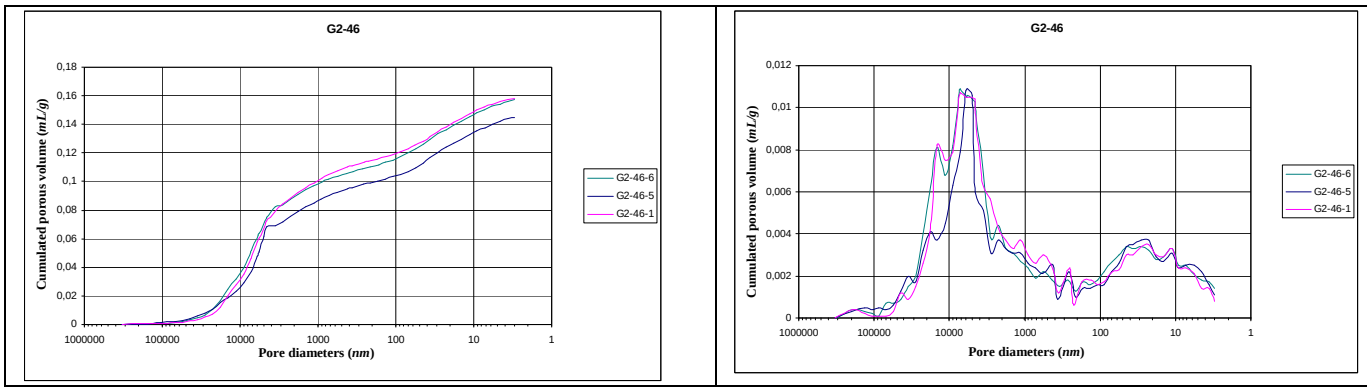


FIGURE 24: MERCURY-POROSITY RANGE OF ACTIVE SAMPLES OF THE G2 REFLECTOR

Pore-size distributions in relation to helium-accessible porosity are shown in Table 29 for moderator graphite and in Table 30 for reflector graphite, respectively. It should be noted that very small diameters (<0.1 µm) are not taken into account in the distribution calculations, as mentioned before.

| Samples | >30 µm | 1-30 µm | From 0.1 to 1 µm | Max. pore diameter (µm) |
|---|---|---|---|---|
| **Virgin** | **3±2.2%** | **75±4%** | **19±0.4%** | **3.4±0.7** |
| G2-27-1 | 7% | 80% | 14% | 5.0 |
| G2-27-7 | 7% | 80% | 13% | 6.3 |
| G2-27-8 | 4% | 83% | 14% | 6.0 |
| **Average** | **6±2%** | **83±0.3%** | **14±0.3%** | **5.7±0.7** |
| G2-32-1 | 2% | 83% | 15% | 5.1 |
| G2-32-6 | 2% | 86% | 13% | 5.9 |
| G2-32-7 | 3% | 82% | 15% | 5.1 |
| **Average** | **2±0.6%** | **84±1.8%** | **14±1.1%** | **5.4 ±0.5** |
| G2-42-1 | 12% | 69% | 20% | 4.7 |
| G2-42-6 | 3% | 78% | 18% | 4.6 |
| G2-42-7 | 6% | 77% | 17% | 3.6 |
| **Average** | **7±2.9%** | **75±7.9%** | **18±0.5%** | **4.3±0.6** |

TABLE 29: RESULTS OF POROSITY MEASUREMENTS OF THE IRRADIATED G2 GRAPHITE MODERATOR

| Samples | >30 µm | 1-30 µm | from 0.1 to 1 µm | Max pore diameter (*µm*) |
|---|---|---|---|---|
| Raw [8] | | | | **2 µm** |
| G2-46-1 | 2% | 84% | 14% | 7.4 |
| G2-46-5 | 5% | 79% | 16% | 6.0 |
| G2-46-6 | 3% | 84% | 12% | 7.2 |
| **Average** | **4±1,0%** | **83±4,5%** | **14±1,0%** | **6,9±0,8** |

TABLE 30: RESULTS FROM POROSITY MEASUREMENTS OF THE IRRADIATED GRAPHITE G2 REFLECTOR

Helium porosimetry detects a modification in the structure of graphite, as illustrated in Figure 25, for moderator samples. Only the curves achieved by the samples resulting from the middle of each core were reported.

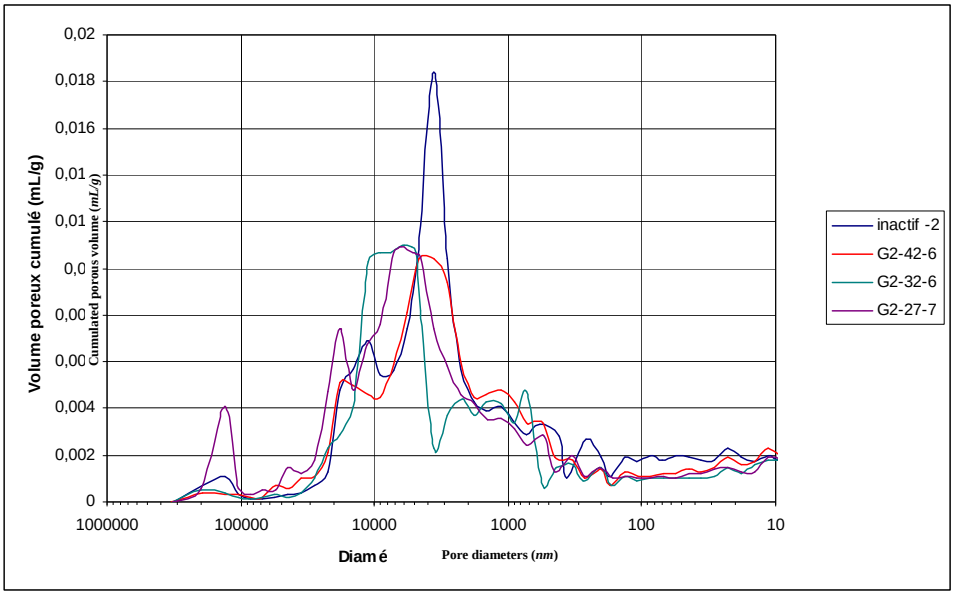


FIGURE 25: PORE-WATER DISTRIBUTIONS FOR IRRADIATED AND VIRGIN GRAPHITE SAMPLES FROM THE G2-REACTOR MODERATOR

A general increase of the macroporosity is observed (pore diameters ranging between 1 and 30 µm) with a wider pore-size distribution mostly for samples G2-27 (68% porosity) and G2-32 (72% porosity) with a modification of the average pore radius in the distribution. The average radius increases from 3.5 µm on inactive samples to 4.3 µm on sample No. G2-42, then further to 5.4 µm for sample No. G2-32, before reaching 5.7 µm for sample No. G2-27. Hence, it may concluded that irradiation induces not only an increase in the average size of graphite pores, but also a modification in the distribution of pore diameters. Those modifications would seem to be due rather to the neutron creeps received by the samples than to temperature, with due account of the small temperature discrepancies between samples.

In the case of reflector graphite, the comparison is only possible on the basis of the available literature. The results displayed in Table 30 show a slight increase in the helium-accessible porosity. The major information seems to be the increase in pore diameters in the field of macroporosity.

## *7.4. X-ray diffraction*

Given the sampling orientation of cores G2-27, G2-32, G2-42 and G2-46 (perpendicularly to the extrusion axis of the brick), the orientation of irradiated samples characterised by X-ray diffraction is identical to that of virgin sample Y3-2 (see Figures 5, 8 and 9). Consequently, the resulting data will be preferentially compared to those resulting from the non-irradiated sample Y3-2. The samples characterised by X-ray diffraction include the following: G2-27-3, G2-32-3, G2-42-3 and G2-46-2. For those four samples, the *a* and *c* meshing parameters and the FWHM of diffraction peaks have been determined.

As in the case for non-irradiated reference samples, X-ray diffraction recordings are representative of Fact Sheet ICDD No. 74-2330 relating to graphite (Annex 1) and display for all characterised samples a significant dissymmetry in the diffraction peaks at small 2θ angles, notably for the main peak (002) (Figure 26). It is worth recalling that such dissymmetry is due to the low density of the graphite, since X rays penetrate deeply inside the samples, thus inducing an asymmetrical widening of the diffraction peaks (absorption effect).

The resulting diffractograms also prove that the crystallographic texture of the moderator samples (Nos. G2-27 à G2-42) is identical to that of sample No. Y3-2. With regard to irradiated sample No. G2-46-2 collected from the reflector, however, it is worth noting the slightly different texture, where the intensities of the peaks correspond to graphene planes [peaks (002), (004) and (006)] and are relatively lower than those for the other peaks. That means that the orientation of coke grains in the extrusion sense is less marked for reflector graphite than for moderator graphite. That phenomenon is consistent with the fact that graphite with a Lockport-coke base is more isotropic than graphite with a "Special" Grade-A base (Table 31).

| **Reactor** | **G1** | ***G2*** | |
|---|---|---|---|
| **Coke** | **Special B** | **Special A** | **Lockport L** |
| **Density** | 1.61 | 1.71 | 1.68 |
| **CTE (// dir.) (25-525°C) ($10^{-6}$ $K^{-1}$)** | 1.44 | 1.25 | 2.68 |
| **Anisotropy coefficient α(⊥) / α(//)** | 2.3 | **2.3** | **1.3** |
| **CTE (⊥ dir.) (25-525°C) ($10^{-6}$ $K^{-1}$)** | 3.31 | 2.88 | 3.48 |

TABLE 31: PROPERTIES OF G1 AND G2 GRAPHITES

*Dilatation thermal dilatation coefficients (CTE)*

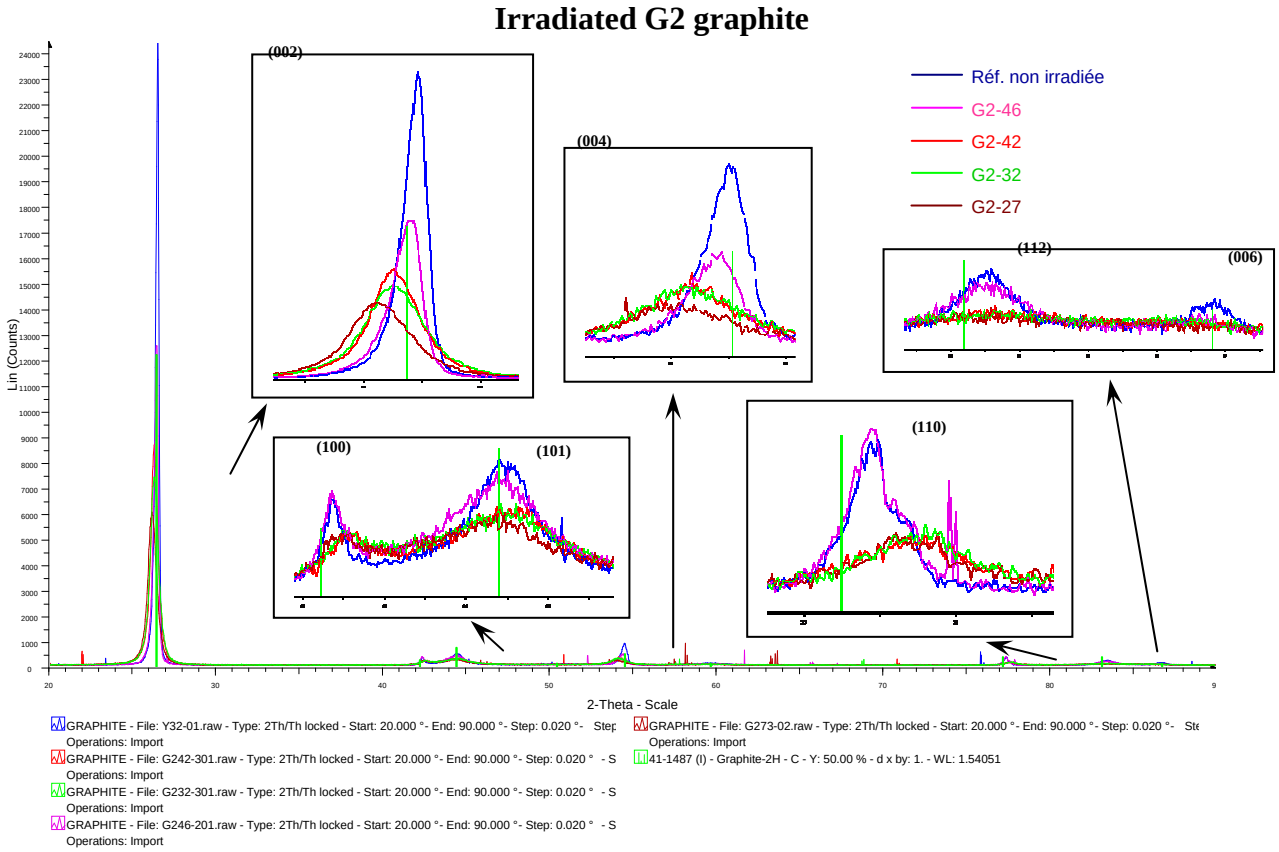


FIGURE 26: DIFFRACTION DIAGRAMS OF IRRADIATED SAMPLES

In Figure 26, the peaks associated with base planes (002), (004) and (006) of the graphite crystal shift towards narrow diffraction angles, thus reflecting an increase of the *c* parameter. Inversely, diffraction peaks associated with prismatic planes (100) and (110) of the graphite crystal shift towards wide diffraction, thus reflecting a decrease of the *a* parameter. The analysis of the recorded diffractograms confirms those initial observations and leads to the meshing parameters presented in Table 32.

| G2 | c parameter (Å) | Δc/c (%) (Ref. Y3-2) | *a* parameter (Å) | Δa/a (%) (Ref. Y3-2) |
|---|---|---|---|---|
| **Theoretical parameters** | 6.707 | NA | 2.461 ± 0.002 | NA |
| **Non-irradiated referenceY3-2 (⊥)** | 6.725 ± 0.002 | NA | 2.460 ± 0.002 | NA |
| **G2-27-3** | 6.805 ± 0.002 | 1.19 ± 0.06 | 2.454 ± 0.002 | -0.24 ± 0.16 |
| **G2-32-3** | 6.777 ± 0.002 | 0.77 ± 0.06 | 2.454 ± 0.002 | -0.24 ± 0.16 |
| **G2-42-3** | 6.775 ± 0.002 | 0.74 ± 0.06 | 2.454 ± 0.002 | -0.24 ± 0.16 |
| **G2-46-2** | 6.745 ± 0.002 | 0.29 ± 0.07 | 2.463 ± 0.002 | 0.12 ± 0.16 |

TABLE 32: MESHING PARAMETERS OF IRRADIATED G2 SAMPLES

Variations in crystalline *a* and *c* parameters are consistent with literature data[18], that is, an increase of *c* and a decrease of *a* under irradiation. Those dimensional variations of graphite crystallites are directly associated with the creation/migration of defects due to neutron irradiation. Neutrons move the carbon atoms of the graphite crystal, which leads to the creation of carbon atoms in pores (increase of the *c* parameter) and the creation of gaps in graphene planes (decrease of the *a* parameter) – see Figure 27. Since the bonds between graphene planes are much weaker than inside the planes, the creation of irradiation defects leads to a much more significant evolution of the *c* parameter than of the *a* parameter.

The evolution of crystalline parameters depends on the number of defects being created and, hence, on the neutron creep and the irradiation temperature. As creep increases, the parameters are modified proportionally up to a threshold value beyond which defects will recombine and cease to participate in the modification of crystalline parameters. Similarly, the higher the irradiation temperature is, the more the defects will be mobile and tend to recombine, thus inducing a lesser effect on the variation of crystalline parameters (Figure 28).

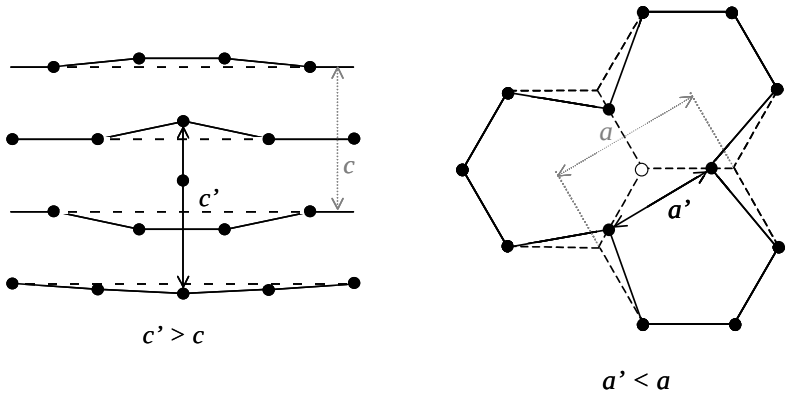


FIGURE 27: IRRADIATION-INDUCED VARIATIONS IN CRYSTALLINE PARAMETERS

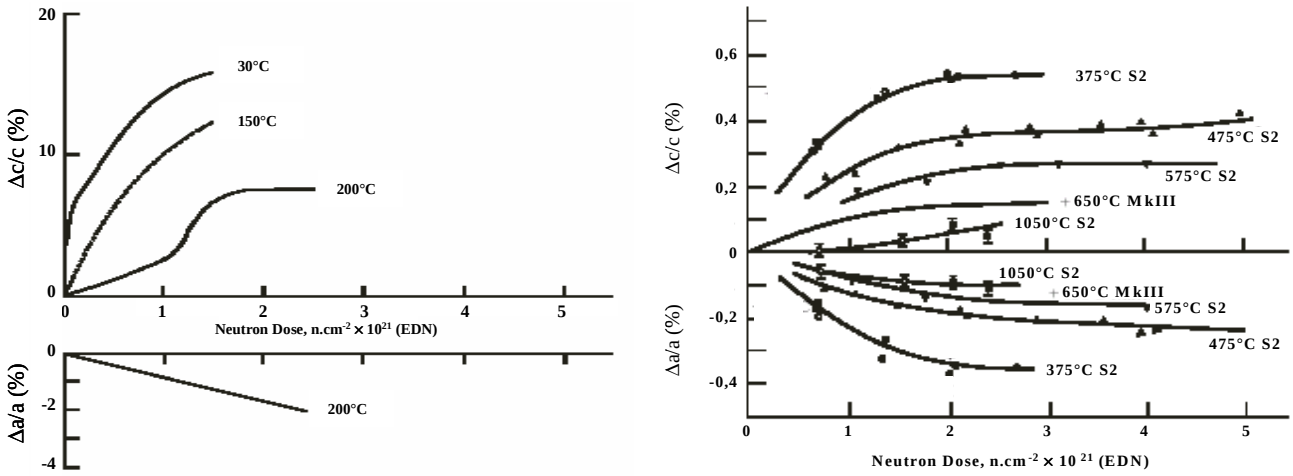


FIGURE 28: VARIATIONS IN *a* AND *c* CRYSTALLINE-GRAPHITE PARAMETERS OF UNDER IRRADIATION AT DIFFERENT TEMPERATURES AND GRAPHITE GRADES [19] P.54-55

With regard to irradiated G2 samples, the modification in the *c* crystalline parameter is all the more significant that the sample is collected from a zone that is close to the pile centre, where creep is more important. Since variations are less sensitive in the case of the *a* parameter, it is not possible to detect any effect of the irradiation gradient, except for sample G2-46-2, whose parameter is comparable to that of the non-irradiated reference (apart from uncertainties). However, that last remark is to be taken cautiously, since the samples are not fully comparable (Lockport coke for G2-46-2 and "Special" Grade-A coke for reference Y3-2).

The analysis of the diffractograms of irradiated G2 samples also led to the FWHMs of diffraction peaks (002), (004) and (110), as shown in Table 33.

| Peak | Reference Y3-2 (FWHM) | G2-27-3 | | G2-32-3 | | G2-42-3 | | G2-46-2 | |
|---|---|---|---|---|---|---|---|---|---|
| | | FWHM | ΔFWHM | FWHM | ΔFWHM | FWHM | ΔFWHM | FWHM | ΔFWHM |
| **(002)** | 0.31 | 0.6 | ***0.29*** | 0.58 | ***0.27*** | 0.46 | ***0.15*** | 0.29 | ***-0.02*** |
| **(004)** | 0.45 | 0.98 | ***0.53*** | 0.94 | ***0.49*** | 0.88 | ***0.43*** | 0.5 | ***0.05*** |
| **(110)** | 0.33 | 0.82 | ***0.49*** | 0.79 | ***0.46*** | 0.78 | ***0.45*** | 0.33 | ***0.00*** |

TABLE 33: FWHM OF DIFFRACTION PEAKS OF IRRADIATED G2 SAMPLES

The purpose of studying the FWHMs of diffraction peaks between irradiated and reference graphite samples was to estimate the modifications in the dimensions of graphite crystallites under irradiation. In fact, in addition to modifying the crystalline parameters of graphite, neutron irradiation may also lead to a significant modification in the height and width of crystallites within coke grains, since those modifications are partly responsible for macroscopic variations in graphite blocks. ΔXa/Xa and ΔXc/Xc deformations, which are associated with the $L_c$ and $L_a$ dimensions of the crystallites and depend on creep and irradiation temperature, are similar to the variations in meshing parameters, but always higher or equal to those variations (Figure 29). In fact, the orderly association of carbon atoms in pores forms new graphitic planes, thus inducing an increase of the crystallites in the *c* direction, whereas, locally, the associated meshing parameter returns to its initial value. As for the creation of gap loops, it generates a contraction along the *a* axis (Figure 30).

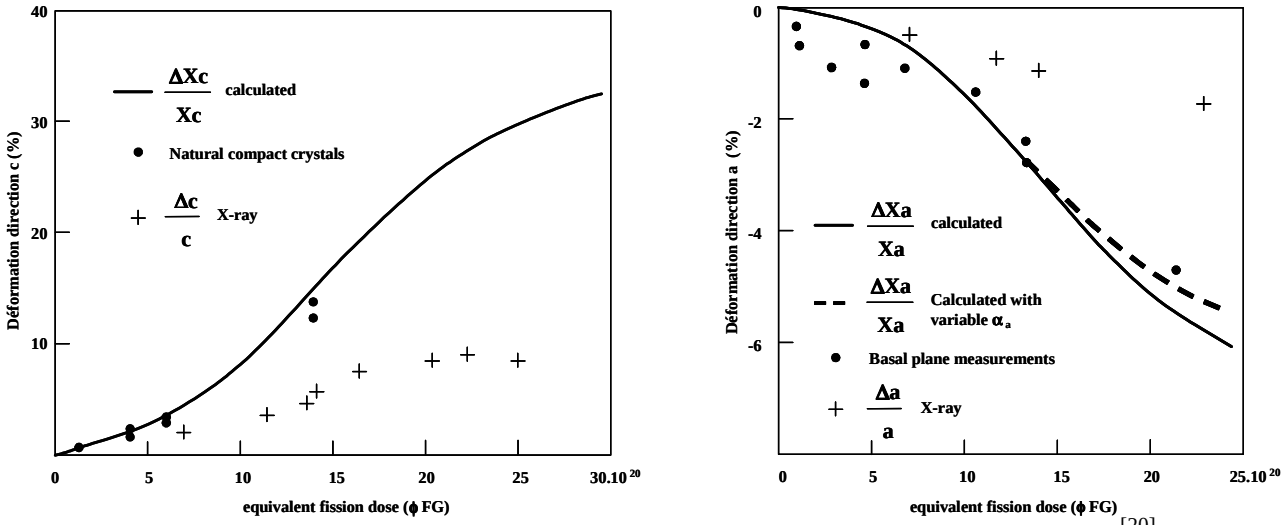


FIGURE 29: EVOLUTION OF THE SIZE OF GRAPHITE CRYSTALLITES UNDER IRRADIATION [20]

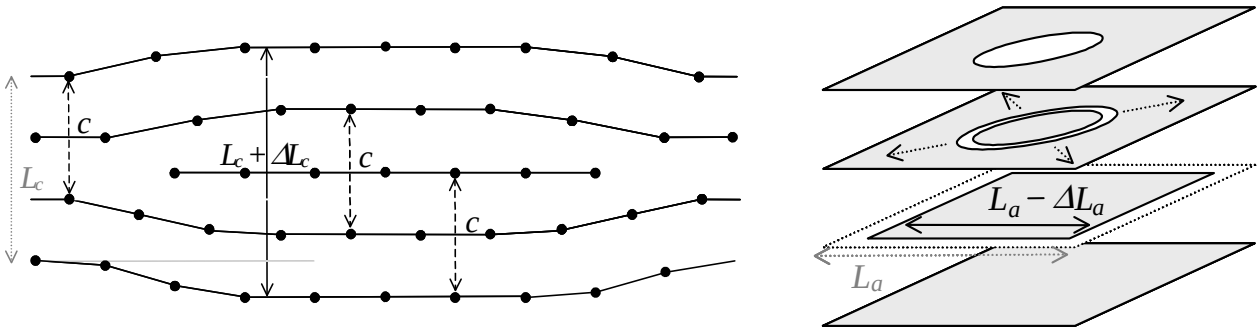


FIGURE 30: VARIATION IN THE SIZE OF GRAPHITE CRYSTALLITES

On one diffractogram, the widening of the diffraction peaks has three sources (11): one instrumental ($H_0$, common to all samples), another associated with the dimensions of the crystallites and grains that diffract ($H_l$), and the last ($H_g$) associated with the presence of microdeformations within the crystallites (presence of defects), as follows :

$$H = H_0 + H_l + H_g \qquad (11)$$

By using Scherrer's formula, it is possible in general to estimate the variation in the size of crystallites and gains within a material (12), as follows :

$$H_l = \frac{k\lambda}{\tau \cos\theta} \qquad (12)$$

where : $H_l$ is the widening in radians of the diffraction peak concerned

$k$ is equal to 0.89, if the FWHM of diffraction peaks is used

$\lambda$ is the wavelength of X-rays (*in metres*)

$\tau$ is the variation in the average size of crystallites in the direction concerned (*in metres*)

$\theta$ is the diffraction angle of the peak concerned

In the case of graphite, the increase in the size of the crystallites in the *c* direction must normally be reflected by a refinement of diffraction peaks (002), (004) and (006) and a decrease in the *a* direction, as well as a widening of diffraction peaks (100) and (110). However, according to the results shown in Table 33, all diffraction peaks have widened significantly, and all the more since the samples are located closer to the pile centre (higher creep). That result reflects the fact that the contribution of microdeformations (associated with defect concentration, $H_g$) in the widening of diffraction peaks is more important and hides the "refining" contribution ($H_l$) of diffraction peaks (002), (004) and (006), which is due to the increase in the *c* direction of the crystallites. Due to the fact that it is impossible to de-correlate $H_g$ and $H_l$ contributions, it is not possible to estimate the increase of crystallites in the *c* direction la direction and their contraction in the *a* direction.

Since the evolution in the FWHMs of diffraction peaks reflect mostly the concentration of crystalline defects in the graphite, the results shown in Table 33 are therefore consistent with the relative position of samples in the G2 pile and confirm the results achieved with crystalline parameters, that is the presence of a gradient of the macrostructural properties from the pile centre (moderator) to the reflector.

## 7.5. Raman spectroscopy

Due to technical reasons relating to connection problems between the nuclearised microscope and the optical fibre connected to the spectrometer, it was impossible to perform the Raman characterisation of the G2 graphite, except on the non-irradiated reference samples. Without proper analyses, it is still not possible today to decide whether carboxyhydrogenated deposits are present or not at the surface of the channels of G2 graphite bricks.

## 7.6. Summary of measurements on irradiated samples

Measurements relating to density and open, sealed, as well as total porosimetry, detected a decrease in density and, consequently, an increase in the total porosity of the most irradiated samples. That difference is highlighted by an increase in density from the edge to the centre of the irradiated samples, whereas the impregnation phenomenon during fabrication and measurements show that the density of inactive samples is higher on the edge than in the centre. The observation is therefore made that profiles are reversed after irradiation. The phenomenon responsible for those differences is radiolytic corrosion, which was more significant towards the edge (due to the contact with gas) than within the samples. As always for samples resulting from the most irradiated zones, the total and open porosities increased, while the sealed porosity decreased. Helium-intrusion measurements show that the average pore diameters had increased mostly in the macroporosity zone. Measurements by X-ray diffraction also show that variations in crystalline parameters are more significant for both moderator-centre samples (increase of the *c* parameter of the mesh and of the FWHM of diffraction peaks).

In the case of the sample located at the reflector/moderator interface, irradiation effects are difficult to quantify and it is therefore possible to estimate that they are negligible from the standpoint of the graphite structure (density, wear and porosity, whether total, open or sealed). Only an increase in the diameter of the pores is observed, as well as a slight evolution in the density within the core. Measurements by X-ray diffraction show a modification in the meshing parameters and smaller FWHMs in diffraction peaks than for the other two samples.

For the reflector sample, conclusions are more difficult to establish due to the absence of any reference sample. However, the measured values in comparison to those found in the literature seem to indicate that variations do not exceed measurement uncertainties. It is therefore possible to conclude to the quasi-absence of irradiation damages on that sample.

# 8 Summary and conclusions

In the framework of the studies on the disposal of “graphite” waste resulting from the UNGG system, it is necessary to obtain reliable data on the behaviour of long-lived radionuclides 36Cl and 14C, with due account of their mobility within the geological medium associated with their long radioactive half-life. The characterisation of the evolution of the structural and microstructural properties of G2 graphite under irradiation forms an integral part of that framework, since it constitutes one of the essential parameters that will have a broad impact on the physicochemical processes that control the release of radionuclides in solution.

From the characterisation of G2 virgin samples, the following observations were made:

– a significant density heterogeneity of the material at the scale of centimetric samples;
– the existence of density gradient between the core and the edge of the brick, which occurred during the less thorough impregnation of graphite at the core of the material;
– porosity is essentially open (22-30%), whereas sealed porosity remains scarce with approximately 3-4%, and
– pore distribution has a significant fraction of pores measuring between 1 and 30 µm (about 75%), with the maximum distribution at 3.5 µm.

Irradiated samples collected during the radial-vertical coring campaign in the G2 reactor in 1989 were also characterised. In general, irradiation induced a small modification in the characteristics of graphite, with due account of the resulting power (260 MW over 22 years) and of the moderate operating temperatures (<250-310°C for the characterised samples). The maximum wear rate reaches only 5% locally on the edges of the most irradiated samples.

The following observations are also made :

- a decrease in density, associated with an increase of the open porosity and a decrease of the sealed porosity, which is all the more important since the sample was irradiated;
- a larger decrease in density on the edges of the brick, which is logically associated with the phenomenon of radiolytic corrosion;
- an increase of the open porosity, which relates essentially to the macroporosity, and
- an increase of both the *c* meshing perimeter and of the FWHM of X-ray diffraction peaks, thus illustrating the increase in structural disorders due to irradiation, which is all the more significant since neutron creep is high.

Characterisations by Raman spectroscopy remain to be performed on irradiated samples in order to complete the study.

All characterisations performed on virgin and irradiated samples were instrumental in providing basic data on the material and, especially, on the porous network. Those data are essential for conducting studies relating to the behaviour of radionuclides under disposal conditions.

Those characterisations are also under way on virgin and irradiated graphite samples from the Saint-Laurent-des-Eaux NPP and will form the subject of a future document.

# LIST OF TABLES

# LIST OF FIGURES

## REFERENCES

[1] Comportement des radionucléides dans les graphites UNGG en milieu aqueux / Synthèse bibliographique et proposition de programme. NT SA3C/LARC 08/02. C. Pichon.

[2] Empilement graphite des réacteurs G2/G3 situation au 1er mars 1978 – Documents Cogéma Marcoule section G2/G3 – (DOCMAN C.19-13 et C.19-14).

[3] Technique de l'ingénieur/génie nucléaire/ modérateurs graphite. P. Cornuault.

[4] Évolution des densités apparentes du graphite pendant les campagnes de production de G2-G3, NT DPC/SCP/CPh/59 -631/Jr/Jb du 21/09/1956 – J. Rappeneau – (DOCMAN C.108.08)

[5] Densités apparentes sur barres entières Valeurs moyennes de la production G2-G3. NT DPC/SCP (DOCMAN C.108.06)

[6] Comparaison des mesures MIREILLE et ZOE pour le graphite d'EDF2. SEC/F_60/27. H.Vidal, 1960 (DOCMAN C.22.06)

[7] Propriétés physiques des graphites nucléaires. M. Bocquet, J. Rappeneau, (DOCMAN C.23.18).

[8] Texture poreuse de nouveaux type de graphites M. Yvars et coll., NT DPC/SCP/SPMN 67-28/JR/CP , 1967, (DOCMAN C.73.06)

[9] Conditionnement pour le stockage définitif des briques de graphite radioactif provenant du déclassement des réacteurs. J.-R Coste et coll., CCE, Science et techniques nucléaire, 1990 EUR 12815,

[10] Actualisation des connaissances radiologiques sur le graphite du réacteur G2 Validation de la modélisation. C. Beker, CEA/DCC/UDIN/EAp NT 90/050 du 03/04/90 (DOCMAN C.19.05)

[11] Conditionnement de graphite de cœur de réacteur, compte rendu des travaux menés sur les carottes de graphites extraites du cœur de G2 en préalable aux tests de lixiviation. H. Vidal et coll, NT SDFMA/SETED-89-115-FA 4823.

[12] Report following the agreement for the exchange of irradiated graphite sample and leaching data between the United States Department of Energy and the Commissarait à l'énergie atomique. J.-R. Coste.

[13] Lixiviation des empilements Graphite de G2 – Comportement des radio-nucléides ($^{36}Cl$, $^{14}C$, $^{3}H$, …) NT SA3C/LARC NT 07-02, C. Guy, J. Comte, 2007

[14] Répartition de température dans l'empilement de graphite des piles G2 et G3 en fonctionnement normal A l'Homme – F Mauracq – NT CEA : DEDR/DEMT/EMT/78/155 (DOCMAN C.19.12)

[15] Détermination des densités réelles des graphites nucléaires. NT CEA/DPC/PCA/SPMN/68-238-PM/CP. Mottet, M. Yvars, Ph. Gerlinger 1968 (DOCMAN 6824).

[16] Effet Wigner dans le graphite. 1966 (DOCMAN C.40.11).

[17] Effets des rayonnements neutroniques sur la porosité des graphites. M. Yvars, P. Mottet, J. Sailleau, 1966 (DOCMAN 6603).

[18] Le graphite dans les réacteurs à haute température 2e partie : le comportement du graphite sous irradiation. L. Gosmain, J.-P. Bonal, 2005 (DOCMAN C.140.11).

[19] Irradiation damage in graphite due to fast neutrons in fission and fusion systems. IAEA TECDOC 1154, April 2000.

[20] D'après P.R. Goggin, R.W. Henson, A.J. Perks, W.N. Reynolds. Carbon, Vol. 1, p. 189, 1964.

# ANNEX 1: ICDD's graphite fact sheet

74-2330 Wavelength= 1.54060 C

C

Carbon

Graphite

Rad.: CuKa1 λ: 1.54060 Filter: d-sp: Calculated

Cut off: 17.7 Int.: Calculated I/Icor.: 10.41

Ref: Calculated from ICSD using POWD-12++, (1997)
Ref: Nixon, D.E., Parry, G.S., Ubbelohde, A.R., Proc. R. Soc. London, Ser. A, 291, 324 (1966)

Sys.: Orthorhombic S.G.: $Cmc2_1$ (36)

a: 2.46 b: 4.26 c: 28.96 A: 0.5775 C: 6.7981

α: β: γ: Z: 24 mp:

Ref: Ibid.

Dx: 1.577 Dm: ICSD # : 028419

Peak height intensity. R-factor: 0.133. C.D. Cell: a=4.260, b=28.960, c=2.460, a/b=0.1471, c/b=0.0849, S.G.=Bb21m(36). PSC: oC24. Mwt: 12.01. Volume[CD]: 303.49.

| 2θ | Int | h | k | l | 2θ | Int | h | k | l |
|---|---|---|---|---|---|---|---|---|---|
| 6.099 | 999* | 0 | 0 | 2 | 49.613 | 2 | 0 | 2 | 8 |
| 12.215 | 115 | 0 | 0 | 4 | 50.375 | 4 | 0 | 0 | 16 |
| 18.366 | 4 | 0 | 0 | 6 | 51.399 | 1 | 1 | 1 | 9 |
| 24.572 | 127 | 0 | 0 | 8 | 51.399 | 1 | 0 | 2 | 9 |
| 30.851 | 33 | 0 | 0 | 10 | 53.344 | 1 | 1 | 1 | 10 |
| 37.227 | 1 | 0 | 0 | 12 | 53.344 | 1 | 0 | 2 | 10 |
| 42.396 | 4 | 1 | 1 | 0 | 55.438 | 1 | 1 | 1 | 11 |
| 42.396 | 4 | 0 | 2 | 0 | 55.438 | 1 | 0 | 2 | 11 |
| 42.516 | 4 | 1 | 1 | 1 | 57.211 | 4 | 0 | 0 | 18 |
| 42.516 | 4 | 0 | 2 | 1 | 57.673 | 3 | 1 | 1 | 12 |
| 42.874 | 1 | 1 | 1 | 2 | 57.673 | 3 | 0 | 2 | 12 |
| 42.874 | 1 | 0 | 2 | 2 | 60.041 | 1 | 1 | 1 | 13 |
| 43.467 | 2 | 1 | 1 | 3 | 60.041 | 1 | 0 | 2 | 13 |
| 43.467 | 2 | 0 | 2 | 3 | 62.537 | 2 | 1 | 1 | 14 |
| 43.725 | 1 | 0 | 0 | 14 | 62.537 | 2 | 0 | 2 | 14 |
| 44.286 | 15 | 1 | 1 | 4 | 64.278 | 1 | 0 | 0 | 20 |
| 44.286 | 15 | 0 | 2 | 4 | 65.157 | 1 | 1 | 1 | 15 |
| 45.321 | 2 | 1 | 1 | 5 | 65.157 | 1 | 0 | 2 | 15 |
| 45.321 | 2 | 0 | 2 | 5 | 67.897 | 1 | 1 | 1 | 16 |
| 46.562 | 3 | 1 | 1 | 6 | 67.897 | 1 | 0 | 2 | 16 |
| 46.562 | 3 | 0 | 2 | 6 | 70.757 | 1 | 1 | 1 | 17 |
| 47.997 | 1 | 1 | 1 | 7 | 70.757 | 1 | 0 | 2 | 17 |
| 47.997 | 1 | 0 | 2 | 7 | 71.631 | 1 | 0 | 0 | 22 |
| 49.613 | 2 | 1 | 1 | 8 | 73.737 | 1 | 1 | 1 | 18 |

| 2θ | Int | h | k | l |
|---|---|---|---|---|
| 73.737 | 1 | 0 | 2 | 18 |
| 76.838 | 1 | 1 | 1 | 19 |
| 76.838 | 1 | 0 | 2 | 19 |
| 77.563 | 4 | 2 | 0 | 0 |
| 77.563 | 4 | 1 | 3 | 0 |
| 77.895 | 2 | 2 | 0 | 2 |
| 77.895 | 2 | 1 | 3 | 2 |
| 78.888 | 1 | 2 | 0 | 4 |
| 78.888 | 1 | 1 | 3 | 4 |
| 79.341 | 1 | 0 | 0 | 24 |
| 79.631 | 1 | 1 | 3 | 5 |
| 80.066 | 1 | 1 | 1 | 20 |
| 80.066 | 1 | 0 | 2 | 20 |
| 80.536 | 1 | 2 | 0 | 6 |
| 80.536 | 1 | 1 | 3 | 6 |
| 82.831 | 5 | 2 | 0 | 8 |
| 82.831 | 5 | 1 | 3 | 8 |
| 83.425 | 1 | 1 | 1 | 21 |
| 83.425 | 1 | 0 | 2 | 21 |
| 85.764 | 3 | 2 | 0 | 10 |
| 85.764 | 3 | 1 | 3 | 10 |
| 86.925 | 1 | 1 | 1 | 22 |
| 86.925 | 1 | 0 | 2 | 22 |
| 87.508 | 1 | 1 | 3 | 11 |
| 87.508 | 1 | 0 | 0 | 26 |
| 89.335 | 1 | 1 | 3 | 12 |
| 89.335 | 1 | 2 | 0 | 12 |

## ANNEX 2: Raman ranges for samples X1-1, Y3-2 and Z1-1

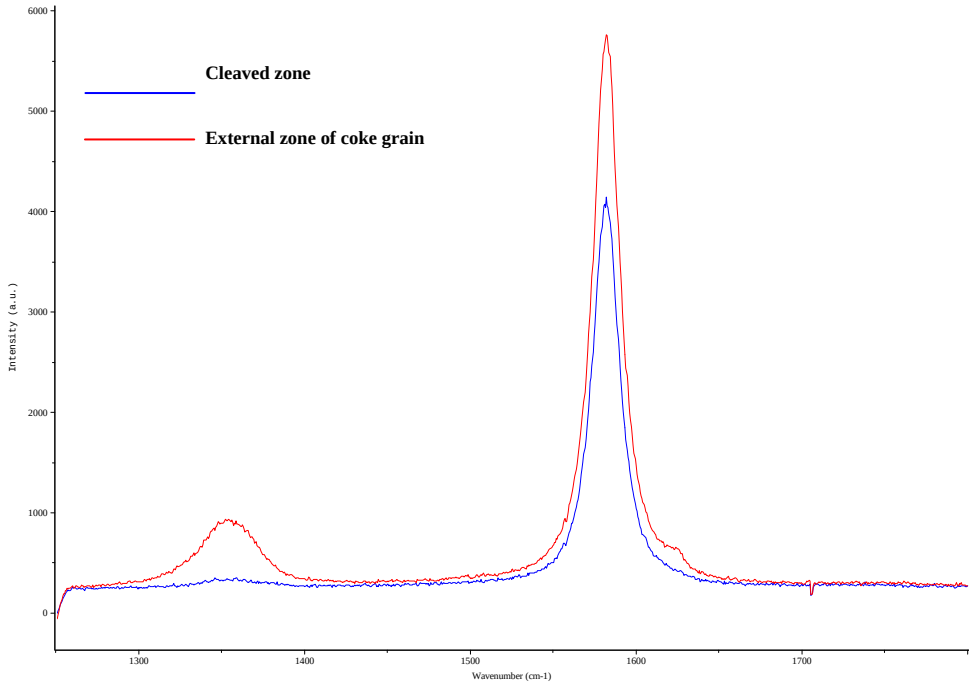


**Raman ranges for sample *échantillons* X1-1**

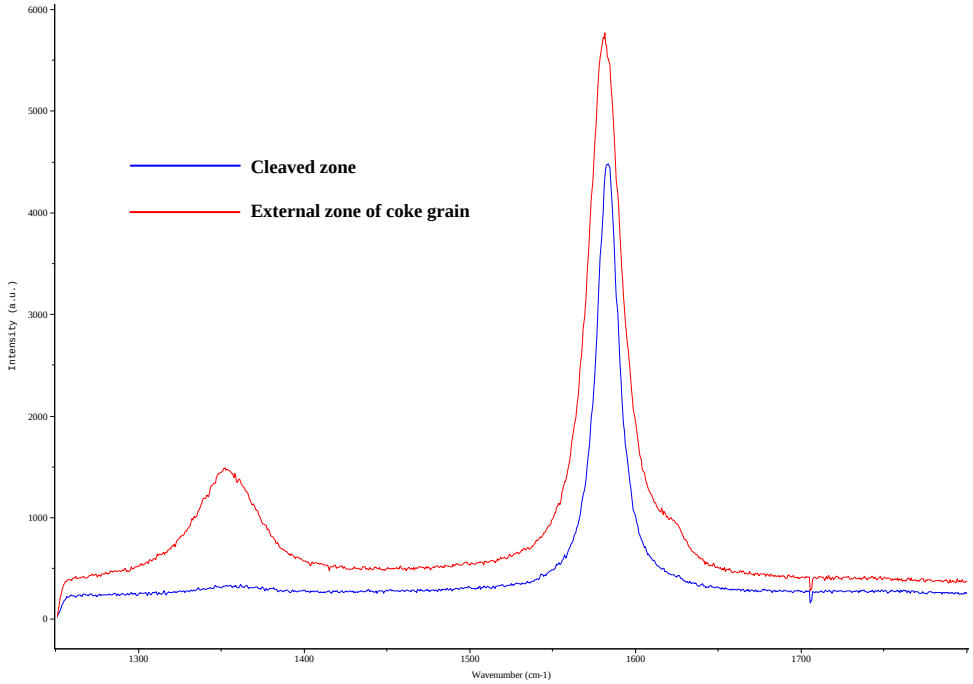


**Raman ranges for sample *échantillons* Y3-2**

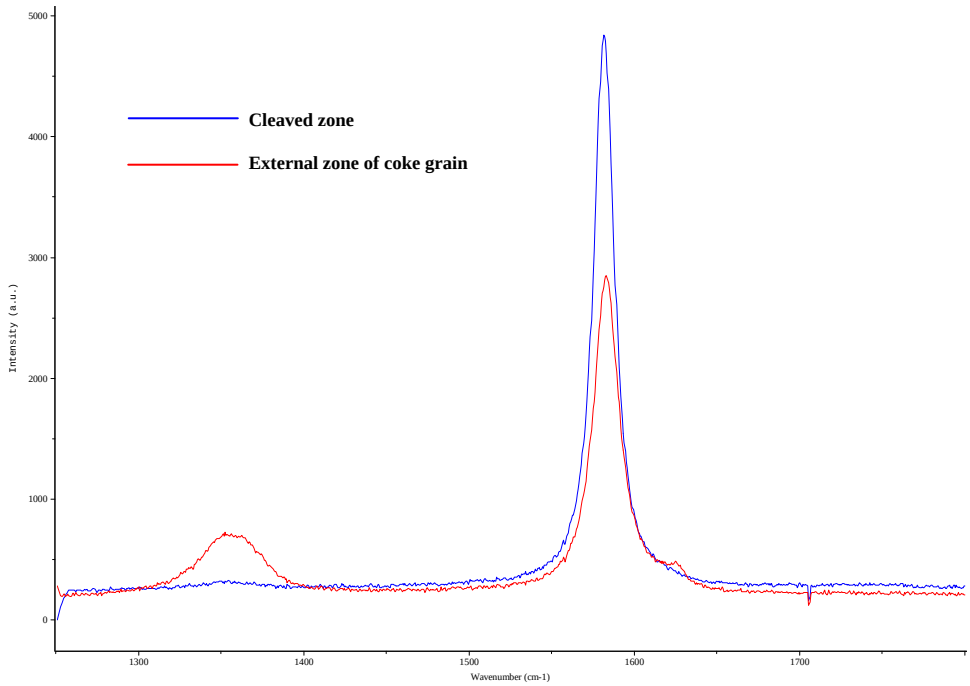


**Raman ranges for sample *échantillons* Z1-1**

## ANNEX 3: Deconvolution of Raman ranges for sample *échantillons* X1-1

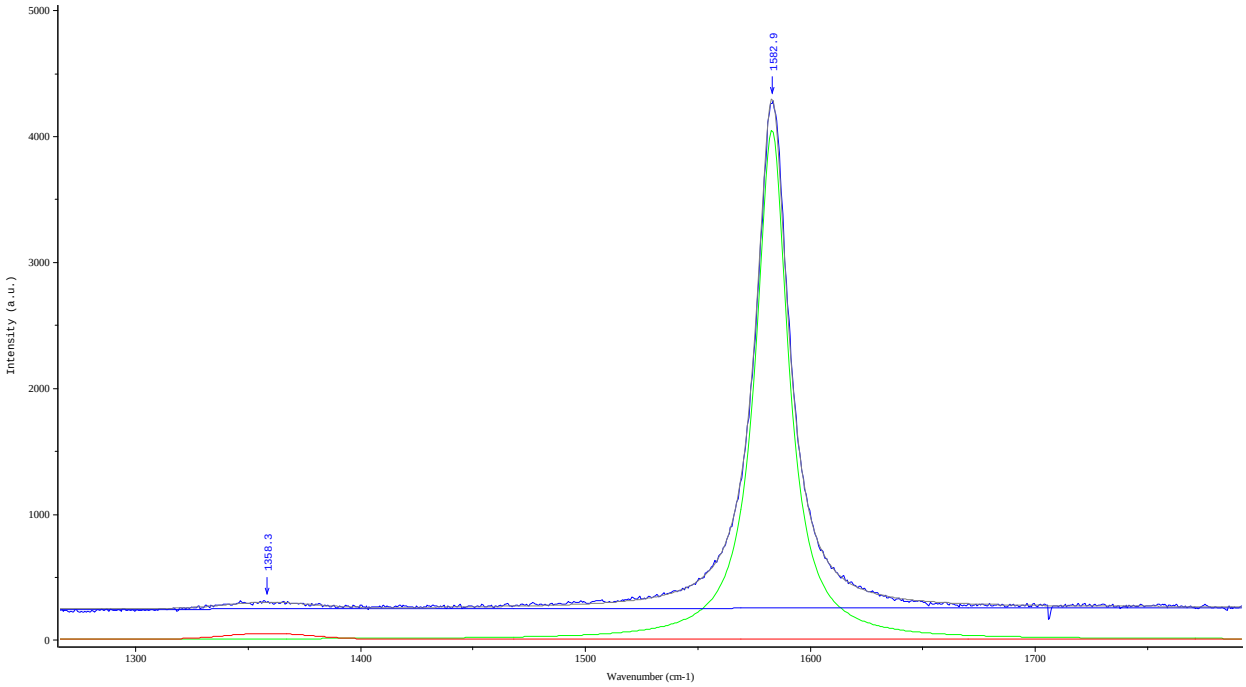


Sample X1-1: Range of the cleaved zone

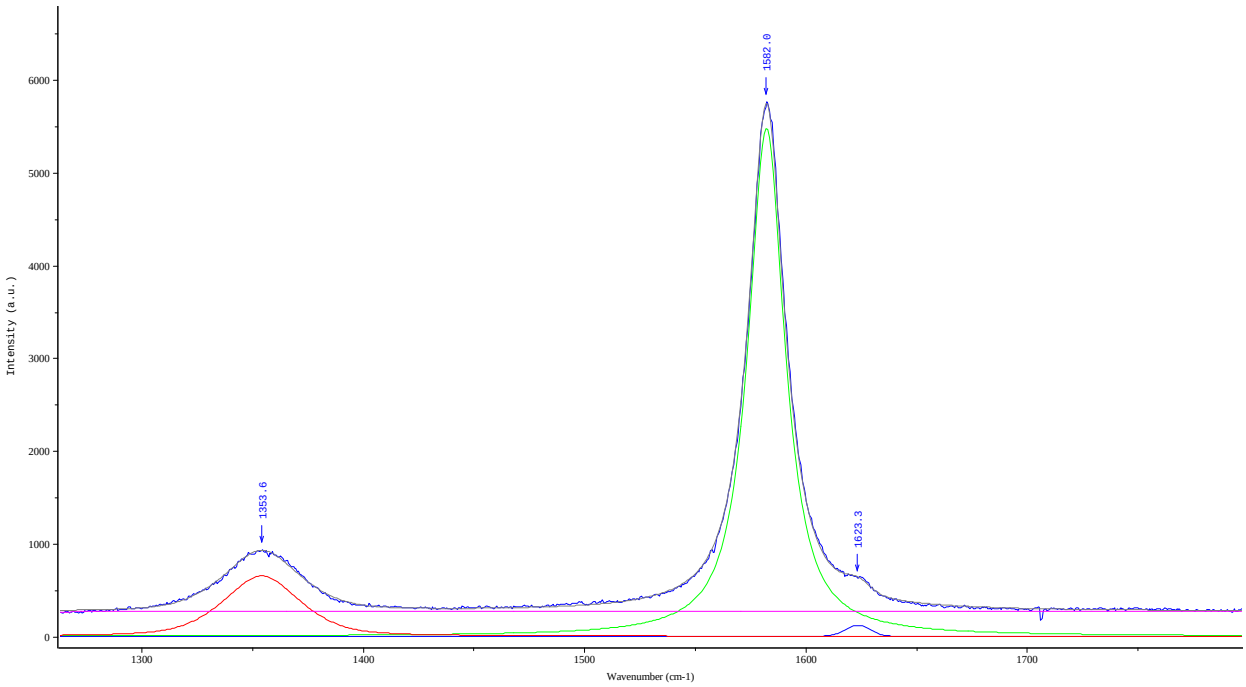


Sample X1-1: Range of the external zone of the coke grain

## ANNEX 4: Deconvolution of Raman ranges for sample *échantillons* Y3-2

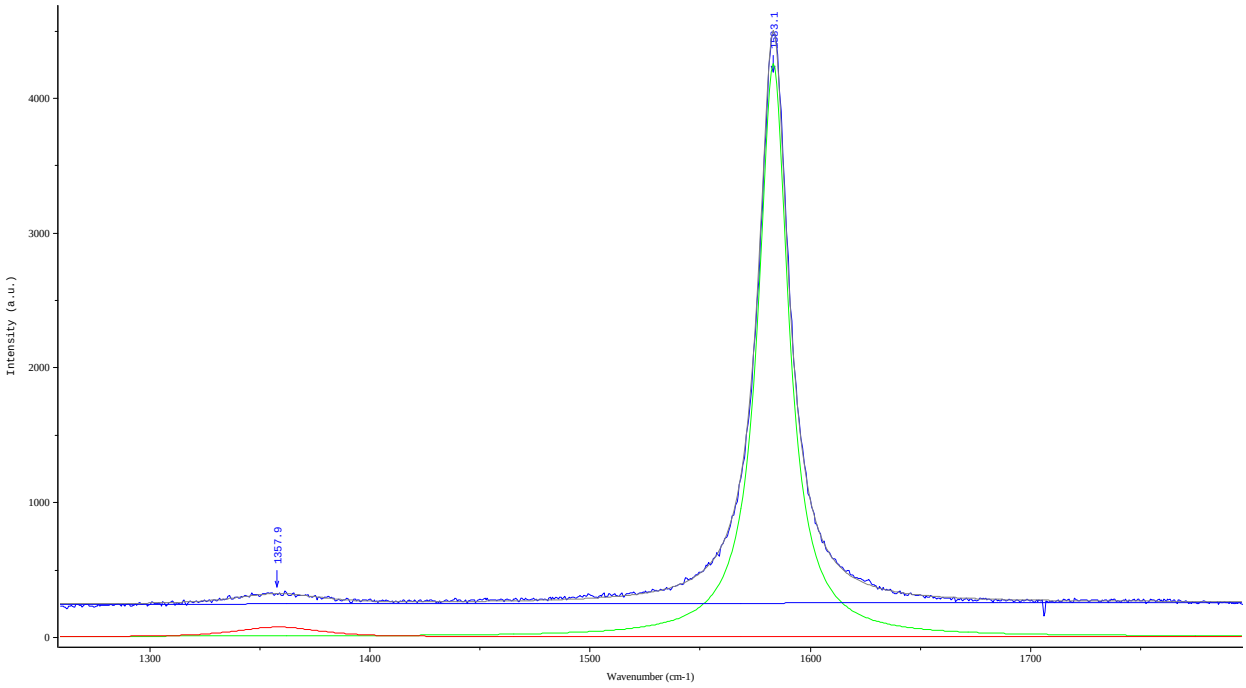


Sample Y3-2: Range of the cleaved zone

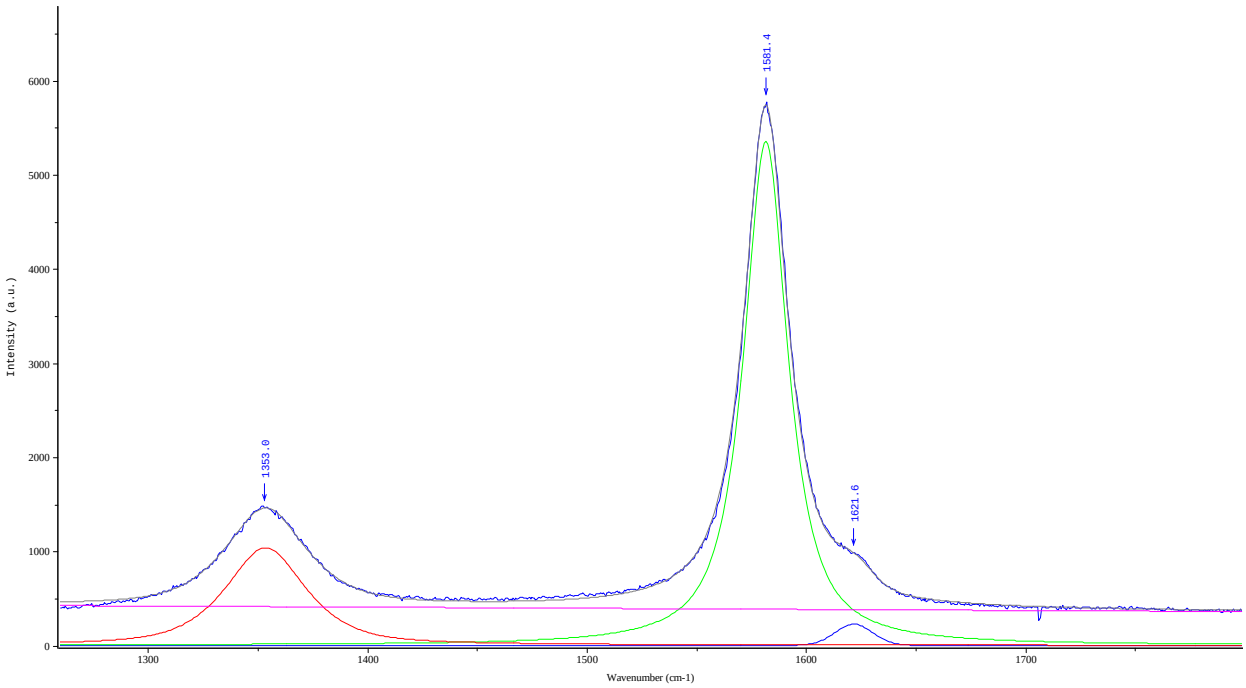


Sample Y3-2: Range of the external zone of the coke grain

## ANNEX 5: Deconvolution of Raman ranges for sample *échantillons* Z1-1

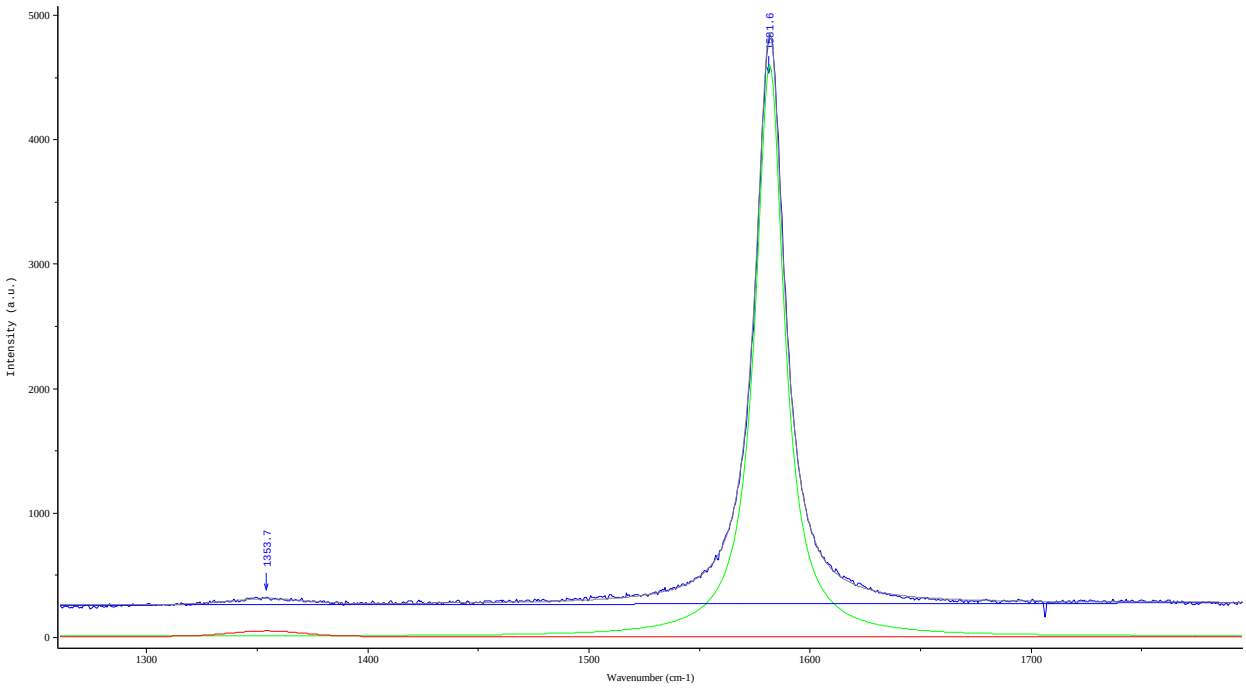


Sample Z1-1: Range of the cleaved zone

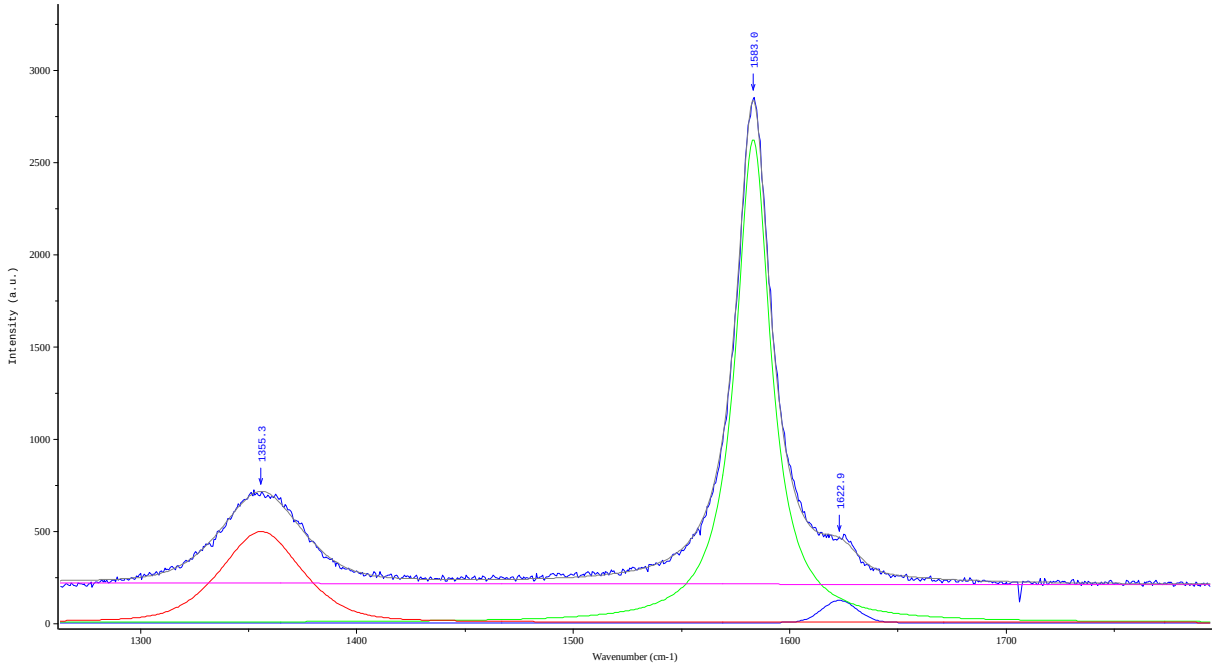


Sample Z1-1: Range of the external zone of the coke grain